CERN/LHCC 2000-009
LEB Status Report/RD48
31 December 1999

3RD RD48 STATUS REPORT

The ROSE Collaboration
(R&d On Silicon for future Experiments)

Co-Spokespersons: Francois Lemeilleur, Gunnar Lindström, Steve Watts

Member Groups:

Bari University, Italy
V. Augelli, M. Angarano, D. Creanza, M. De Palma, L. Schiavulli

Berkeley, University of California, Dept. of Materials Science, USA
E. Weber, H. Feick

Brookhaven National Laboratory, USA
Z. Li, B. Dezillie

Bucharest, Institute of Nuclear Physics and Engineering, Romania
A. Vasilescu

Bucharest, Institute of Physics and Technology of Materials, Romania
T. Botila, D. Petre, I. Pintilie, L. Pintilie, C. Tivarus

Catania University, Italy
S. Albergo, D. Boemi, R. Potenza, A. Tricomi

Centro Nacional de Microelectronica (CNM-CSIC), Barcelona, Spain and
Instituto de Fisica Corpuscular, (IFIC-CISIC), Valencia
F. Campabadal, M.J. Costa, L. Fonseca, J. Fuster, M. Lozano, C. Martinez, J.M. Rafi

CERN, Switzerland
F. Lemeilleur, M. Letheren, M. Glaser, M. Moll, P. Riedler, S. Roe, P. Weilhammer, K. Zankel

Demokritos, Institute of Nuclear Physics, Greece
G. Fanourakis, D. Loukas, A. Markou, I. Siotis, S. Tzamarias, A. Vayaki

Dortmund University, Germany
R. Wunstorf, J. Wüstenfeld

Fermilab, Batavia (IL), USA
S. Kwan, D. Anderson

Firenze University, Italy
M.Bruzzi, U. Biggeri, E.Borchi, E.Catacchini, E. Focardi, G. Parrini

Gent University, Belgium
P. Clauws

Glasgow University, U.K.
K. Smith, R. Bates, S. Manolopoulos, V. Oshea, A. Pickford, C. Raine

Hamburg University, Germany
G. Lindström, E. Fretwurst, M. Kuhnke, M. Moll

Karlsruhe University
W. de Boer, G. Grigoriev, F.Hauler, S. Heising, L. Jungermann

Kiev, Institute for Nuclear Research, Academy of Sciences, Ukraine
P. Litovchenko

Lancaster University, UK
T. Sloan, T. Brodbeck, A. Chilingarov, G. Hughes, P. Ratoff, B.K.Jones

Liverpool University, U.K.
P. Allport, G.Casse, M. Hanlon

London, Brunel University, UK
S. Watts, A. Holmes-Siedle, M. Ahmed, M. Solanky, C. Da Via

London, Imperial College, UK
G. Hall, B. MacEvoy, A. Santocchia

London, Kings College, UK
G. Davies

Ljubljana, J. Stefan Institute, Slovenia
V. Cindro, G. Kramberger, M. Mikuz, D. Zontar

Modena University, Italy
G. Ottaviani

Montreal University, Canada
C. Leroy, P. Roy

Munich, Max Planck Institute, Germany
G. Lutz, R.H. Richter

Padova University, Italy
D. Bisello, N. Bacchetta, J. Wyss

Perugia University, Italy
G.M. Bilei, P. Bartalini, P. Ciampolini, D. Passeri

Pisa, INFN, Italy.
G. Tonelli, R. Dell'Orso, A. Messineo, P. Verdini, R. Wheadon

Prague, Nuclear Center of Charles University
I. Wilhelm

Prague, Czech Technical University, Czech Republic
B. Sopko, S. Pospisil, V.Linhart

Prague, Institute of Physics, Academy of Sciences, Czech Republic
V. Vrba, P. Sicho

Stockholm, Royal Institute of Technology, Sweden
B. Svensson

St Petersburg, Ioffe Physico-Technical Institute, Russia
E. Verbitskaya, V. Eremin, A. Ivanov, I. Ilyashenko

Tel Aviv University, Department of Engineering, Israel
A. Ruzin

Villigen, PSI, Switzerland
K. Gabathuler, R. Horisberger

Warsaw, Institute of Electronic Materials Technology (ITME), Poland
Z. Luczynski, E. Nossarzewska, P. Zabierowski

Warsaw, Institute of Electron Technology (ITE), Poland
M. Wegrzecki, I. Wegrzecki, W. Slysz

Associated Companies:

Canberra Semiconductor, Belgium
P. Burger

Centro Nacional de Microelectronica (CNM-CSIC), Spain M. Lozano

CiS, Erfurt, Germany
K. Stolze

Institute of Electron Technology (ITE), Warsaw, Poland
M. Wegrzecki, I. Wegrzecki, W. Slysz

Institute of Electronic Materials Technology (ITME), Warsaw, Poland
Z. Luczynski, E. Nossarzewska, P. Zabierowski

Micron Semiconductor, U.K.
C. Wilburn

SINTEF, Norway
B. Sundby Avset

Observers:

European Space Agency, ESTEC, Solar System Division, Holland
B. Johlander

IMEC, Belgium
C. Claeys, E. Simoen

Max Planck Institute, Munich, Germany
J. Kemmer, N. Meidinger

EXECUTIVE SUMMARY

This is the third report of the ROSE Collaboration. The Collaboration has existed since October 1995 and was formally approved as RD48 by the LHCC in June 1996. Its objectives are:

a) To develop radiation hard detectors that can operate beyond the limits of present devices and that ensure guaranteed operation for the whole lifetime of the LHC experimental programme.

b) To make recommendations to experiments on the optimum silicon for detectors and quality control procedures required to ensure optimal radiation tolerance.

The Collaboration has performed a systematic evaluation of the effect of oxygen and carbon impurities on the radiation tolerance of silicon detectors.

The key scientific results of the project are:

- The leakage current damage parameter is material independent (no impurity, resistivity or conduction type dependence). It has been linked to defect clusters which are not affected by the material. Annealing of the leakage current is also material independent. The damage parameter and its annealing has been shown to scale ideally with NIEL (non ionising energy loss), i.e. without any remaining particle or energy dependence.
- Effective doping changes can be improved by oxygenation of the material (factor 3) Such improvement is only observed when the radiation environment contains a significant charged particle component. This has been understood in terms of the production of larger numbers of isolated vacancy/interstitial pairs during charged particle irradiation.
- Lower resistivity oxygenated material is beneficial for detectors that operate in a radiation environment dominated by reactor energy neutrons.
- Reverse annealing has been linked to defect clusters. After proton irradiation, this process is found to saturate at high fluence ($\geq 2\ 10^{14} p.cm^{-2}$) for oxygenated silicon. This provides a significant safety margin. In addition, the time constant for the process is found to be a factor 4 larger. This would allow detectors to remain at room temperature for longer periods during maintenance periods and thus offers a substantial safety margin.
- Detailed correlations have been found between microscopic defect formation and macroscopic damage parameters. Defect kinetics models and device models can predict macroscopic behaviour well, even for hadron irradiation.
- A macroscopic damage parameter model has been developed which can be used to predict detector parameters in a given radiation environment. This model has been used already in operational projections for major LHC experiments.

The key technological results of the project are:

- Two methods were found to highly oxygenate silicon. Firstly, at the ingot growing stage. Secondly by diffusion of oxygen into ANY wafer using a high temperature drive-in (a minimum of 16 hours at 1150 ^{O}C seems to be sufficient).
- This technology has been successfully transferred to several silicon detector manufacturers (SINTEF, Micron, ST, CIS) and full-scale microstrip detectors produced.

Results from full scale oxygenated microstrip and pixel detectors are now becoming available. The key results so far are:

- DOFZ (Diffusion Oxygenated Float Zone) wafers produce detectors which prior to irradiation are no different to those produced on standard material.
- Depletion voltage curves derived from signal measurements with LHC speed electronics for irradiated oxygenated strip detectors look to be significantly lower than those on corresponding detectors processed on standard material. However, more data on detectors from a variety of suppliers is urgently required. The degree of improvement looks consistent with results obtained from signal studies on simple diode test structures. Consistency with CV derived depletion voltages requires further investigation.

The following work needs to be performed in the next few months:

- The minimum diffusion time required to give radiation hardening needs further study. The beneficial effect that oxygen has on the reverse annealing process needs more work. As this effect is crucial to the maximum maintenance period that can be used by the experiments, it needs further investigation. This work is extremely time consuming.
- The physics of bulk damage should be the same in full-scale detectors as in simple diodes. Nevertheless, bulk damage parameters should be extracted from irradiated strip detectors and compared to the well-measured parameters obtained with diodes.
- The violation of NIEL by charged hadrons in oxygenated material needs further study. Testing with radiation sources that better represent the environment in the LHC experiments needs to be performed. The neutron spectrum in the LHC experiments extends to much higher energy than for reactor sources. There are good reasons to believe that oxygenated silicon will perform better than standard material in such a neutron environment.

In conclusion, the Collaboration has achieved its main objectives. Diffused oxygen technology has been successfully transferred to the LHC experiment detector groups and industry. Some further work is required to answer the remaining questions.

1. INTRODUCTION

This is the third status report of the RD48 (ROSE) Collaboration. The two earlier ones of 1997 and 1998 are listed as ref. [1] and [2]. Silicon pixel and microstrip detectors have been selected as best choice for most tracking applications in the forthcoming LHC experiments. However the required ten years of safe operability poses an extreme challenge to their radiation hardness, predominantly due to the hadron induced damage in the silicon bulk. The collaboration is concentrating on these problems, performing systematic investigations of all detector relevant effects, including the search for an improved radiation tolerance by special defect engineering methods. The main scientific results are outlined, of which the following two points are of major importance. Oxygen enrichment of the silicon bulk, introduced by RD48 and achieved within the manufacturing process, has resulted in substantial radiation hardening of the devices. Secondly, a model description has been developed allowing reliable predictions of the detector performance for the LHC operational scenario. Based on these results recommendations are outlined concerning the choice of material and detector processing for silicon trackers. This technique has been successfully transferred to several manufacturers and test devices for the large LHC experiments are presently under study in close cooperation with RD48. In addition, considerable progress has been achieved in the understanding of the microscopic processes responsible for the macroscopically observed effects. Finally we will survey the main open questions which still have to be answered regarding several aspects of the macroscopic features pertaining to detector performance.

It should be noted that the results presented in this report reflect the combined continuous effort of all collaborating groups, working together in the preparation and characterisation of test devices, the irradiation experiments, and other related investigations and analysis. The RD48 groups have carried out numerous studies and a proper presentation of all individual results is not possible within the limited scope of this report. Therefore, the illustrations included in this report are necessarily selected in order to show the different effects in the clearest way. In each case references to the relevant papers, technical notes or workshop talks are given. A complete publication list of the collaboration (numbering about 100 papers) is in preparation and will be available shortly on the ROSE web page [8].

The next RD48 workshop will be held at CERN in the beginning of March 2000, when the results given in this report will be discussed in more detail, together with many other findings that have not been mentioned or only been referenced briefly here. This Workshop will also be a platform for a broader discussion with both the detector manufacturers and the tracker groups of the large LHC experiments.

2. THE ROSE COLLABORATION – DEFECT ENGINEERING.

The ROSE Collaboration currently consists of 37 international groups working on detectors for particle physics experiments at the LHC. The Collaboration benefits from the very valuable input of solid state physicists and the expertise of silicon manufacturers, who are also members of RD48. In addition the close involvement of Canberra, CNM, Micron and SINTEF is shown through their "Associated Company" status. Inputs are also acknowledged from the European Space Agency, IMEC, Belgium and the MPI Semiconductor Laboratory in Munich all of which are cooperating via an "Observer" status. Work at ITE and ITME (both RD48 members) has been vital for the rapid development, production and processing of various materials. More recently collaboration with ITME has resulted in high quality material characterisation. Finally the RD48 technique for Oxygen enrichment had been successfully transferred to CiS (Germany), Micron (Great Britain), SINTEF (Norway) and ST-Microelectronics (Italy). These manufacturers have produced dedicated ROSE test detectors and full scale detector prototypes for LHC experimental groups on oxygenated silicon.

The Collaboration formed following the First Workshop on Radiation Hardening of Silicon Detectors at CERN in October 1995. The proposal [3] was approved by the LHCC in June 1996. The Second Workshop was held at CERN in February 1997 [4], the third one at DESY in February 1998 [5] and the fourth at CERN in December 1998 [6] followed by a Meeting in June 1999 [7]. As noted above, the Fifth Workshop will be held shortly in March 2000. A World-Wide-Web page also provides useful information [8].

The objectives of the collaboration are:

- The development of radiation hard silicon detectors that can operate beyond the limits of present devices and that ensure guaranteed operation for the whole lifetime of the LHC experimental programme.

- The outline of recommendations to experiments on the optimum silicon for detectors and quality control procedures required to ensure optimal radiation tolerance.

The key idea is that one can improve the radiation tolerance of silicon by defect engineering. Defect engineering involves the deliberate addition of impurities to silicon in order to affect the formation of electrically active defect centres and thus control the macroscopic parameters of devices. According to current models RD48 had relied on oxygen and carbon as the key ingredients for a possible change in the radiation hardness. Oxygen and carbon capture silicon vacancies and interstitials respectively. The carbon is converted from a substitutional to an interstitial position which is mobile at room temperature. It eventually forms stable defects with oxygen and substitutional carbon. Migrating silicon interstitials and vacancies escape from a region of silicon where an intense concentration of Frenkel pairs are produced by a Primary Knock-On Atom (PKA). The PKA is produced by the incident radiation. Vacancies can react with one another to form multivacancy defects. This leads to clustering of intrinsic defects especially at the end of the PKA range. This so-called "cluster" region controls many of the electrical parameters of irradiated silicon.

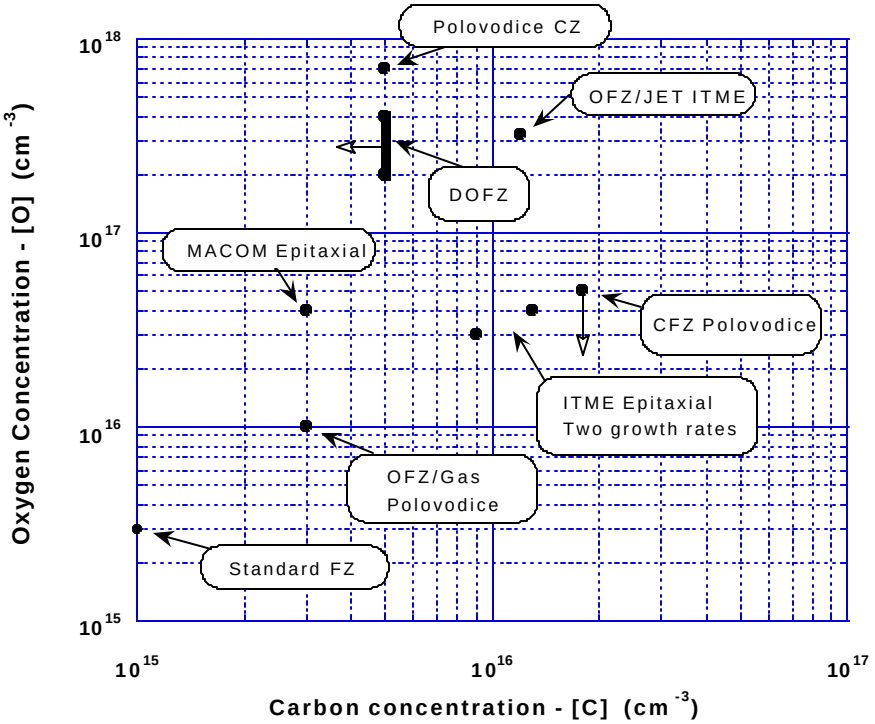

Fig.1: Oxygen and carbon concentrations in substrates investigated by the ROSE Collaboration.

Various types of silicon have been investigated in the past, covering most of the accessible phase space in Carbon and Oxygen concentration, see Fig.1. The important role of Oxygen was first demonstrated by the use of Czochralski (Cz) silicon, where concentrations of up to 10^{18} cm^{-3} are normal due to the growing process in a Quartz crucible. However this material is not available in detector grade quality and the results were hence of limited value. The use of epitaxial silicon was also investigated. In this case O-diffusion from the Oxygen rich Cz substrate leads to an appreciable enhancement of the O-concentration with respect to standard FZ (Float Zone) silicon. The results obtained with such test devices, with a thickness of up to 200 μm, were encouraging but were not pursued further because the cost of production was not suitable for mass application. Gas doping during the FZ growing of the silicon ingot was first applied by Polovodice in Prague but they could not get concentrations higher than about 10^{16} cm^{-3}. ITME in Warsaw then grew highly oxygenated silicon using a gas jet technique during the FZ process, achieving an O-concentration of up to $3\ 10^{17}$ cm^{-3}. A method which results in the same enrichment but has a substantially higher cost effectiveness was finally initiated by RD48 and carried out by ITE. The technique consists of diffusion of oxygen from a thick oxide layer grown via a prolonged oxidation step. It should be mentioned that this had been invented originally several years ago by BNL but did not lead to any sizeable enhancement of the radiation tolerance [9].

The initial RD48 tests on neutron damage with this material were at first also discouraging. It was only in the second half of 1998 that the CERN group found an appreciable hardening effect both by using jet oxygenation and O-diffusion processed detectors following proton induced damage. Possible reasons for the difference between charged hadron and neutron damage will be discussed later. The success demonstrated in the 1998 workshop [6] then led to the fast transfer of the O-diffusion technique to various manufacturing companies, of which SINTEF was the first one, followed later on in 1999 and likewise successful by CiS and ST-Microelectronics. Micron also used a modified technique, using an O-implanted layer as the supply for the succeeding diffusion throughout the bulk. Because of the success obtained with the O-enriched detectors, other possibilities for radiation hardening were not pursued anymore in the past year. Among those alternatives which would be very interesting is the Sn-enrichment of silicon. Ref. [10] shows that tin highly suppresses divacancy production. Both Topsil and ITME have grown Sn-doped FZ silicon achieving a Sn-concentration of 2 to $3\ 10^{17}$ cm^{-3}. A future investigation of such material could also help in clarifying the role of Oxygen in the hardening process.

The proper characterisation of the material before exposing the detectors to radiation damage was vital for our investigations. Secondary Ion Mass Spectroscopy (SIMS) has proven to be the most reliable technique for evaluating the O-concentration profiles. In Fig. 2 an example is shown comparing the depth profile of Oxygen after standard oxidation with the result obtained in a high temperature long term diffusion process, performed at BNL [11]. The homogeneity of the [O]-profile is extremely flat and the concentration of $4\ 10^{17}$ cm^{-3} is by far the highest yet achieved with this technique. In this case a dedicated Quartz tube was used, allowing for continuous tempering at 1200°C but in routine production lines the temperature is limited to 1150°C. This limitation can be overcome by using a SiC tube instead and the results obtained this way have shown to

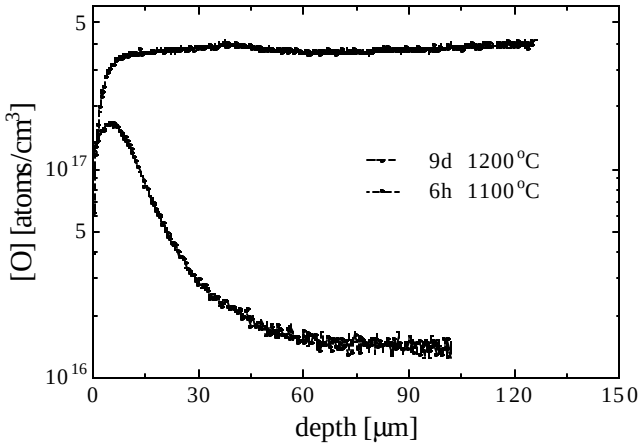

Fig.2: Oxygen-concentration profiles for standard and oxygen enriched FZ silicon wafers as measured by SIMS.

be very comparable to those reached with a standard Quartz oven.

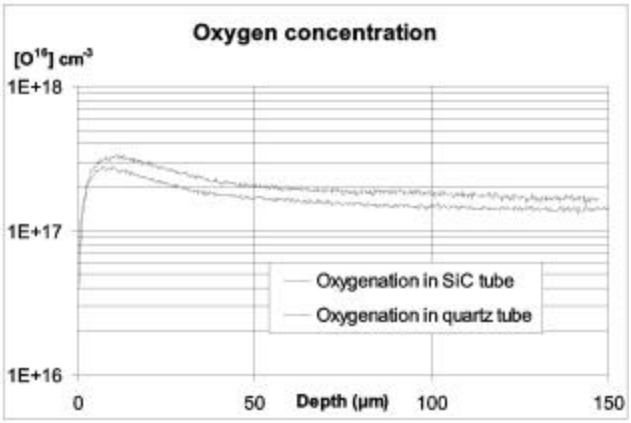

Fig.3: Oxygen concentration depth profiles.

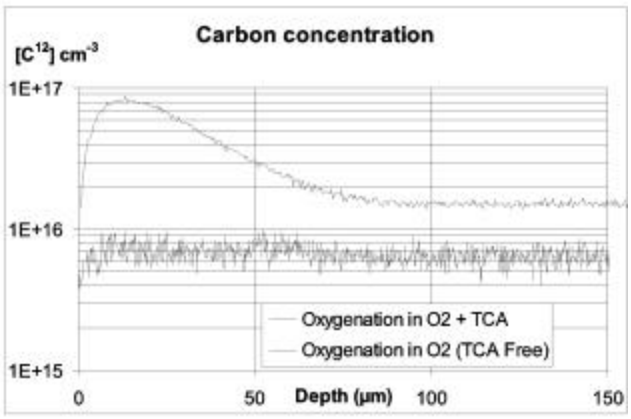

Fig.4: Carbon concentration depth profiles.

The results shown in Fig.3 have been obtained by a cooperation between SINTEF and CNM. One of the key questions is how much O-enrichment is really necessary and how can that be obtained. A short diffusion of not more than 16 hours at 1150°C ([O] = 1.5 10^{17} cm^{-3}) may already be enough for the required radiation hardening effect. This point of optimisation is under further study. In contrast to the improvement gained by O-enrichment, an increased Carbon-concentration does have an adverse effect. Hence it is reassuring that diffusion in a SiC tube does not enhance the C-contribution in the silicon bulk. While TCA (a Carbon containing compound) is used in helping the normal oxidation process it must be strictly avoided during the O-diffusion process - see Fig.4 (same source as for Fig.3). The best process now in wide use is a standard oxidation followed by diffusion in a Nitrogen atmosphere. Another point of worry is whether the RD48 oxygenation process changes the resistivity of the bulk material or has any other adverse effect. A resistivity profile before and after oxygenation is shown in Fig.5, contributed by ITE. No appreciable change of the resistivity or its homogeneity throughout the depth of the wafer is detected. Finally detectors produced by this method show a similarly low bulk current as those following standard processes. This has been convincingly demonstrated e.g. by SINTEF where the I/V characteristics have shown suitable high voltage stability and a current at room temperature of about 5 $nAcm^{-3}$ at 4 times the depletion voltage!

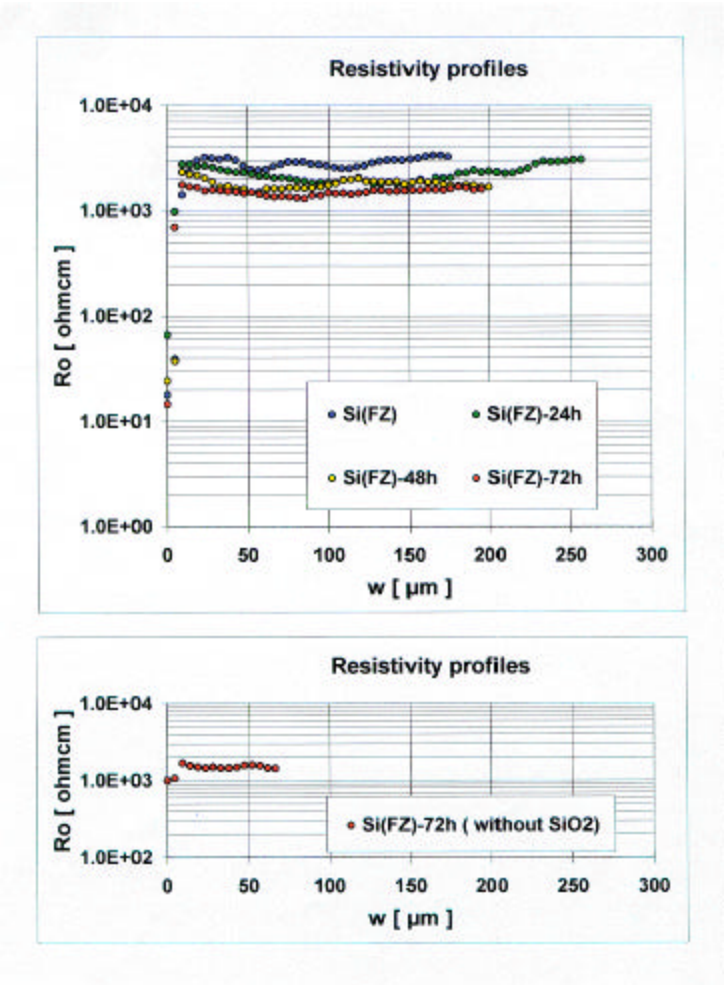

Fig.5: Resistivity depth profiles of standard and oxygen enriched wafers originating from the same ingot.

All materials used for the experiments covered in this report were standard FZ silicon of both <111> as well as <100>

orientation and resistivity between 1 and 15 kΩcm, supplied by Polovodice, Topsil and Wacker. Different enrichment processes have been used, either during the FZ growing or the detector processing stage. Prior to irradiation the detectors have fully been characterised as to their resistivity and as to the O- and C-concentration.

3. MACROSCOPIC EFFECTS –BASIC FEATURES

This section provides a brief overview of radiation effects in silicon detectors to make the document self contained and provide a proper reference for the results given in the later sections.

Three main macroscopic effects are seen in high-resistivity diodes following energetic hadron irradiation, these are:

- Change of the doping concentration with severe consequences for the operating voltage needed for total depletion.
- Fluence proportional increase in the leakage current, caused by creation of recombination/generation centres
- Deterioration of charge collection efficiency due to charge carrier trapping leading eventually to a reduction in the signal height produced by mip's.

The second and third effect have consequences to the S/N ratio for mip's. However trapping has been found to be tolerable and the reverse current can be largely reduced by operating the detectors at a moderately reduced temperature of about -10°C. The first effect is the most severe, as the operating voltage cannot be increased to very high values. This limitation is predominantly set by the diode processing, but note that a large operating voltage together with the increased reverse current leads also to an increase of dissipation power which may affect the cooling system, and if distributed nonhomogenously could also lead to thermal run away effects. Details of these basic damage produced deterioration effects have been described in [2]. However the following important points should be repeated.

NIEL-scaling and irradiation sources

Detectors to be used in the LHC trackers will have a thickness of between 250 and 300 μm and they are processed on 1 to 5 kΩcm mostly n-type silicon wafers. The radiation effects to be encountered depend in principal on the particle type and energy. However, macroscopic changes normally scale with the Non Ionising Energy Loss (NIEL). For the leakage current increase this scaling has recently been verified using different kinds of silicon material as will be shown later. Exceptions from this rule have been found when comparing the effect that neutron and charged hadron damage have on the effective doping concentration. However, in order to get a good perception on what could be expected from different particles and energies the folding of a given energy distribution with the relevant NIEL function gives quite reliable results. The differences observed from charged or neutral hadrons are then projected onto the parameters describing the radiation effects, see later. A compilation of recommended NIEL values for different particles in the whole relevant energy range can be found in [12]. It is common practice to represent the intensity of any hadron irradiation by its equivalent fluence of 1 MeV neutrons. All results in this report are given as function of these F_{eq}-values. The different sources are then characterised by a so called hardness factor k, describing the damage efficiency of a particular source. The hardness factor is defined by $k = F_{eq}/F_{tot}$ with F_{tot} being the total measured particle fluence. For the inner detector tracking regions pions and neutrons are the most relevant hadrons. Consequently RD48 test-experiments have been performed with monoenergetic (PTB Braunschweig) and reactor neutrons (energy ranging to about 10 MeV, TRIGA type reactor at Josef Stefan Institute Ljubljana), 200 MeV pions (PSI Villigen) and 24GeV/c protons (CERN

PS). The proton irradiation facility at CERN [13] has been widely used to represent the effects of charged hadrons in comparison to neutrons.

Effective Doping Concentration and Depletion Voltage

Under reverse bias the electric field in a silicon diode extends from the p^+n junction through the n-type silicon bulk and the total field depth (depletion depth) increases with increasing voltage. The bias value causing the electric field to finally reach through the total depth of the diode is called the depletion voltage V_{dep}. This value depends on the diode thickness d and the effective doping concentration N_{eff} in the following way:

$$(1)\quad V_{dep} = \frac{q_0}{2\varepsilon\varepsilon_0}\left|N_{eff}\right| d^2$$

This equation holds not only for the original n-type silicon with N_{eff} governed by an abundance of donors but also after severe irradiation when the effective doping concentration changes its sign, due both to a removal of donors and the increasing generation of acceptor like defects. In any case $|N_{eff}| = |N_d - N_a|$, with N_d being the donor-concentration and N_a that of the acceptors. Especially for the original material it is useful to remember the relation between the specific resistivity ρ, the doping concentration N_{eff} and the depletion voltage V_{dep}.:

$$(2)\quad N_{eff} = \left(q_0 \mu_{n,p} \rho_{n,p}\right)^{-1}; \qquad V_{dep} = \frac{d^2}{2\varepsilon\varepsilon_0 \mu_{n,p} \rho_{n,p}}$$

Here $\mu_{n,p}$ denotes the mobility of electrons and holes in *n* or *p-type* material.

In addition to an instantaneous change in the effective doping concentration (both donor removal and acceptor generation) the silicon bulk exhibits long term annealing effects after irradiation which are beneficial during a short time period but are adverse for very long times. This latter so called reverse annealing has become a point of much concern as it finally limits the operability of the detectors. The long term behaviour depends however, due to the underlying defect kinetics, very strongly on the detector temperature. In fact, the reverse annealing has shown to be efficiently frozen at temperatures below *-10°C*. Hence the LHC experiments will keep their detectors cold during the beam periods for the sake of a reduced reverse current but also for most of the remaining time without beam, in order to reduce the overall reverse annealing effect. Only very short warm up periods of around 2 weeks are foreseen for maintenance each year. A summary of the complex fluence and time dependence of the effective doping concentration is shown schematically in Fig.6.

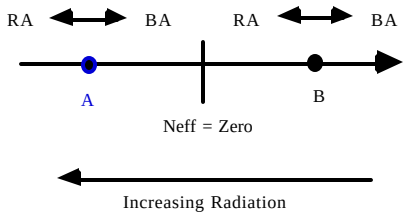

Fig.6: Changes in the effective space charge, N_{eff}, in the depletion region of diodes irradiated by fast neutrons. BA and RA refer to the beneficial and reverse annealing processes that occur after irradiation. N_{eff} is represented as a point on the axis.

Reverse current

The reverse current increase exhibits far less complexity than that observed for the depletion voltage. It is entirely due to the generation of electron/hole-pairs in the silicon bulk. All detectors have guard ring structures in order to guarantee a defined value of the sensitive volume *V* (junction area times detector thickness). Provided a guard ring is used, the measured current *I* is strictly proportional to the volume of the

bulk and it is also proportional to the equivalent irradiation fluence that the detector has received. One therefore defines a *current related damage rate* α by:

(3) $I = \alpha \cdot \Phi_{eq} \cdot V$

The damage induced bulk current decreases strongly with lower operating temperature according to:

(4) $I(T) \propto T^2 \exp\left(-\frac{E_g}{2k_B T}\right)$

where T is the operating temperature, E_g the band gap energy of *1.12 eV* and k_B is the Boltzman constant. Operating the detectors at e.g. *-10°C* reduces the current with respect to its room temperature value by a factor of *20*. Normally the values for the current related damage rate α are given for *20°C* using equation (4). These values can then easily be transferred to any given operating temperature. The damage induced bulk current undergoes also a temperature depending beneficial annealing effect, its universal functional dependence will be shown in section 4.

Charge collection

Bulk damage induces trapping of charge carriers which leads to a deterioration of the charge collection efficiency and thus a reduction in the signal height for mip's. The prime condition for achieving a reasonable charge collection is to establish a sizeable electric field strength throughout the detector. To only apply a bias voltage necessary for total depletion is certainly not enough. In this situation the electric field decreases from its maximum value at the junction side to practically zero level at the opposite electrode. Therefore charge carriers reach zero velocity at that point and consequently the charge collection does not have a finite duration. The trapping probability of any charge carrier during its drift through the detector is proportional to the ratio of the charge collection time t_c and the trapping time constant τ. Hence a large value of t_c/τ must be avoided. For severe damage in the order of 10^{14} -10^{15} cm^{-2} an appreciable overbias may be needed to ensure optimum conditions. Illustrations will be shown in section 4.

4. MACROSCOPIC EFFECTS – LATEST RESULTS

Current related damage rate

As stated in the preceding section, the damage induced increase of the reverse current appears to be of less complexity than those effects responsible for the change in the depletion voltage. In fact, a careful measurement of the current related damage rate α has shown that its value does not depend on any material property so far studied, no matter whether it is *n-* or *p-type* silicon. Likewise it is independent of the resistivity of the silicon and most important of all it is identical for *neutron, proton* and *pion* induced damage and shows no variation with fluence in a range between 10^{11} - 10^{15} *cm*$^{-2}$. This is nicely documented in Fig.7, where the exact fluence proportionality of the volume related current increase at a specific annealing stage is displayed. In fact this behaviour has then led to use of the measured increase of the reverse current for an exact determination of the *1 MeV neutron equivalent fluence* to which the detectors have been irradiated [14]. Equally impressive is the existence of a universal annealing function, again not dependent on material properties, particle type and energy as well as the fluence used for irradiation. The curve representing this function is given in Fig.8 in an example for an annealing temperature of *60°C*. Using the measured parameters governing the temperature dependence, given in [14], one can easily derive the annealing behaviour at any given temperature. It should be emphasised that in contrast to other damage effects, the

functional dependence of a on the annealing duration is exactly the same in Oxygen-enriched and standard material. The method of deriving the equivalent fluence from the measured current increase is therefore considered to be very reliable. Measurements were normally done after 80 minutes annealing at 60 °C resulting in a value of

(5) $a_{80/60} = (3.99 \pm 0.03) \cdot 10^{-17}\, Acm^{-1}$

Using this method for defining the equivalent fluence for a given particle source and comparing it with the otherwise measured total fluence (e.g. by activation analysis of irradiated Al as in case of a high energetic proton beam or Au as for energetic neutrons) hardness factors have been established, see Table 1.

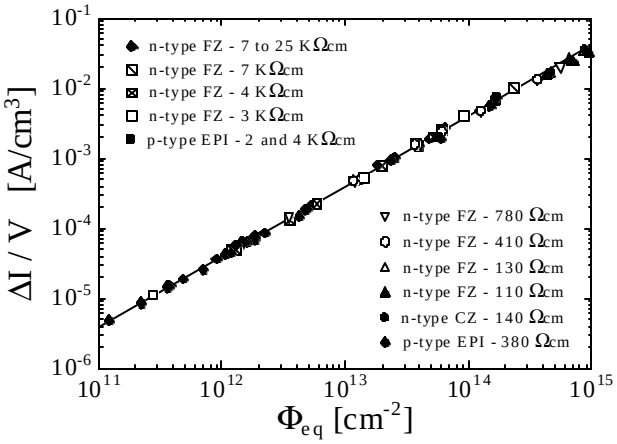

Fig. 7.: Fluence dependence of leakage current for detectors produced by various process technologies from different silicon materials. The current was measured after a heat treatment for 80 min at 60°C [14].

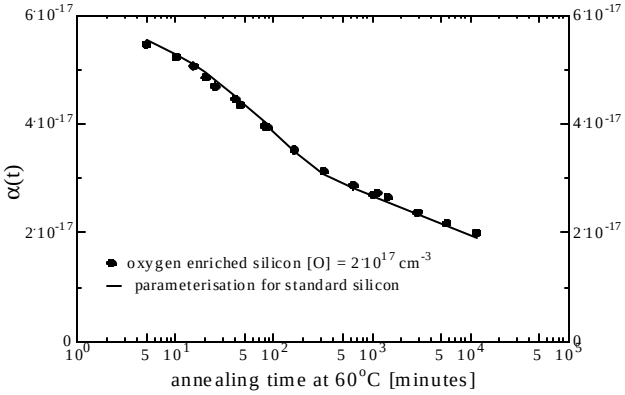

Fig.8: Current related damage rate α as function of cumulated annealing time at 60°C. Comparison between data obtained for oxygen diffused silicon and parameterisation given in Ref. [14].

Table 1.: Hardness factors κ for various sources as determined by the α value and expected from NIEL calculations [12,14, 15].

Irradiation source	Hardness factor κ from α value	Hardness factor κ theoretical expectation (NIEL)
PTB Be(d,n) <En> = 5.2 MeV	(used as reference)	1.45
CERN PS 24 GeV/c protons	0.51 ± 0.01	≈ 0.5
Ljubljana reactor neutrons	0.90 ± 0.05	0.91± 0.05
UKE ^{3}H(d,n) 14.1 MeV n	≈ 1.7	1.80
^{60}Co-gamma	1.9×10^{-6}	6.4×10^{-3}

CERN-scenario measurements for rapid comparisons

As outlined in section 3, the damage induces an instantaneous change of the effective doping concentration as determined from the depletion voltage. The effective doping concentration undergoes a short term beneficial annealing and subsequently a reverse annealing effect on a much longer time scale. Measurements taken immediately after irradiation could be misleading because longer irradiation times would also include some self-annealing and thus the results would depend both on fluence and irradiation time. A much better method consists of consecutive irradiation steps with intermittent short term annealing of *4 minutes at*

80°C and measurement thereafter. This scenario, introduced by the CERN group of RD48 [16] has been found to be extremely useful, since at this stage the change in the effective doping concentration reaches a flat minimum and thus the long term reverse annealing affects the results only slightly. In addition such an annealing is approximately equivalent to 2 weeks at room temperature, a storage time which is foreseen as the yearly maintenance period e.g. in the ATLAS-SCT. The method allows measurements of important damage features as function of fluence almost simultaneously with the ongoing irradiation steps and a comparison between many different diodes can thus be obtained rapidly. At low fluences the change in the effective doping concentration is dominated by donor removal thus leading to a decrease in the full depletion voltage. Once the donor concentration is exhausted or compensated by acceptors, N_{eff} reaches a minimum, at which the conduction type of the material changes from n- to p-type. The introduction rate of negative space charge beyond the inversion point, resulting from the generation of deep acceptors, is called the β-value, defined as the slope of a linear line fit to the data. Fig.9 shows the results of such measurements for standard and Oxygen enriched diodes after irradiation with *neutrons, pions* and *protons*. It can be clearly seen that the oxygen rich material reveals a much lower β-value for *pion* and *proton* irradiation than observed for standard silicon. On the other hand for *neutron* induced damage such an improvement is not visible. Reasons for this different behaviour will be given later. Fig.10 displays data obtained by the same method but compares *standard*, *Carbon-* and *Oxygen-rich* samples, exposed to *proton* irradiation. The improvement of the *O-rich* diodes with respect to standard ones is $\beta_{st}/\beta_{[O]} = 3.5$, while *Carbon-rich* samples show an appreciable worsening by a factor of *3*! It can also be seen from Fig.10, that different diffusion times used in this case for oxygenation do not affect the β-improvement. Two other important features have also been revealed by the CERN-scenario measurements.

Fig.11 and 12 show the results with *O-rich* diodes using silicon of different resistivity. In Fig.11, displaying the proton damage, one deduces that the effective doping concentration reached at high fluences well above inversion point, is independent of the initial resistivity. In terms of our present understanding this means that the removal effect has exhausted the initial donor concentration completely and hence the space charge at larger fluences is only governed by the generation of acceptors. However for neutron irradiation, as shown in Fig.12, the situation is different. At least part of the difference in the initial doping concentration present before irradiation remains available even at a fluence of 2×10^{14} *cm*$^{-2}$. Thus the increase of the acceptor concentration is partly compensated due to this incomplete donor removal. The consequence for the choice of material is then: while using silicon with different resistivity for detectors does not have any effect on the needed depletion voltage at larger fluences following proton irradiation one gets an appreciable beneficial effect for neutron induced damage by choosing O-rich low resistivity material. As an example, *1 kWcm n-type* silicon would result in an initial depletion voltage of *290 V* for a *300 mm* thick diode, whereas for *15 kWcm* one would need only *20 V*. For a donor removal of only *30%* as to be deduced from Fig.12, *70%* of the initial difference in depletion voltage, i.e. *190 V* less voltage would be needed for the *1 kWcm* Oxygen-enriched diode after high fluence.

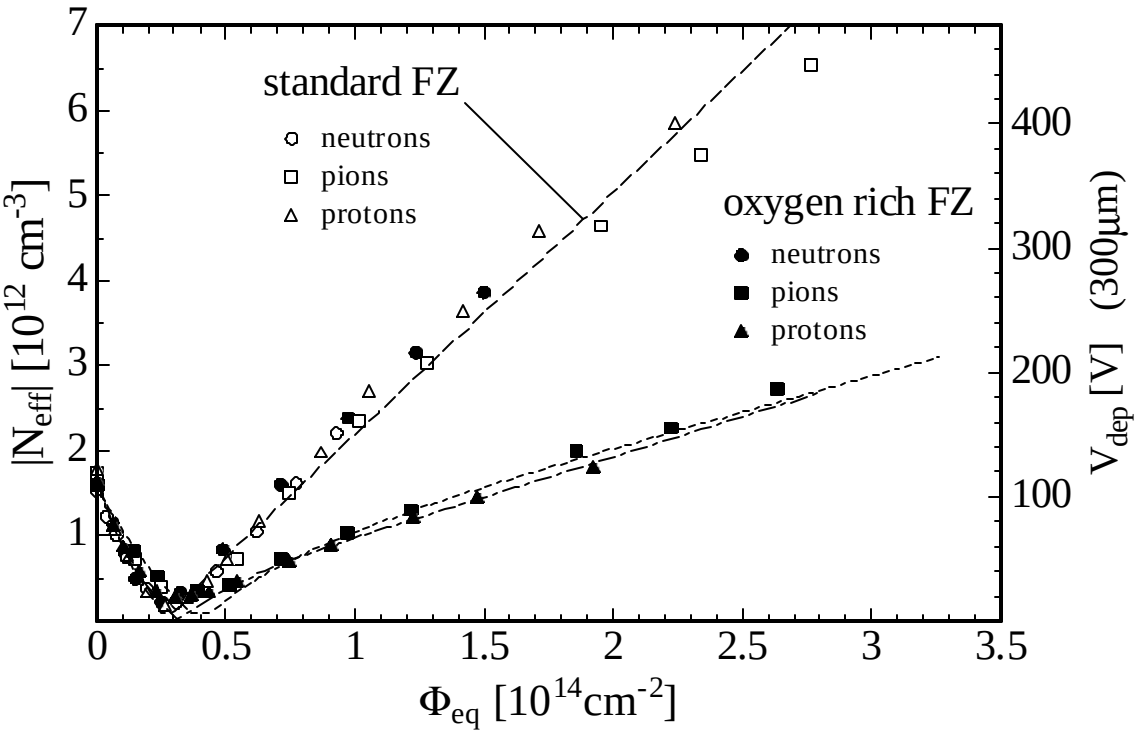

Figure 9: Dependence of N_{eff} on the accumulated 1 MeV neutron equivalent fluence for standard and oxygen enriched FZ silicon irradiated with reactor neutrons (Ljubljana), 23 GeV protons (CERN PS) and 192 MeV pions (PSI).

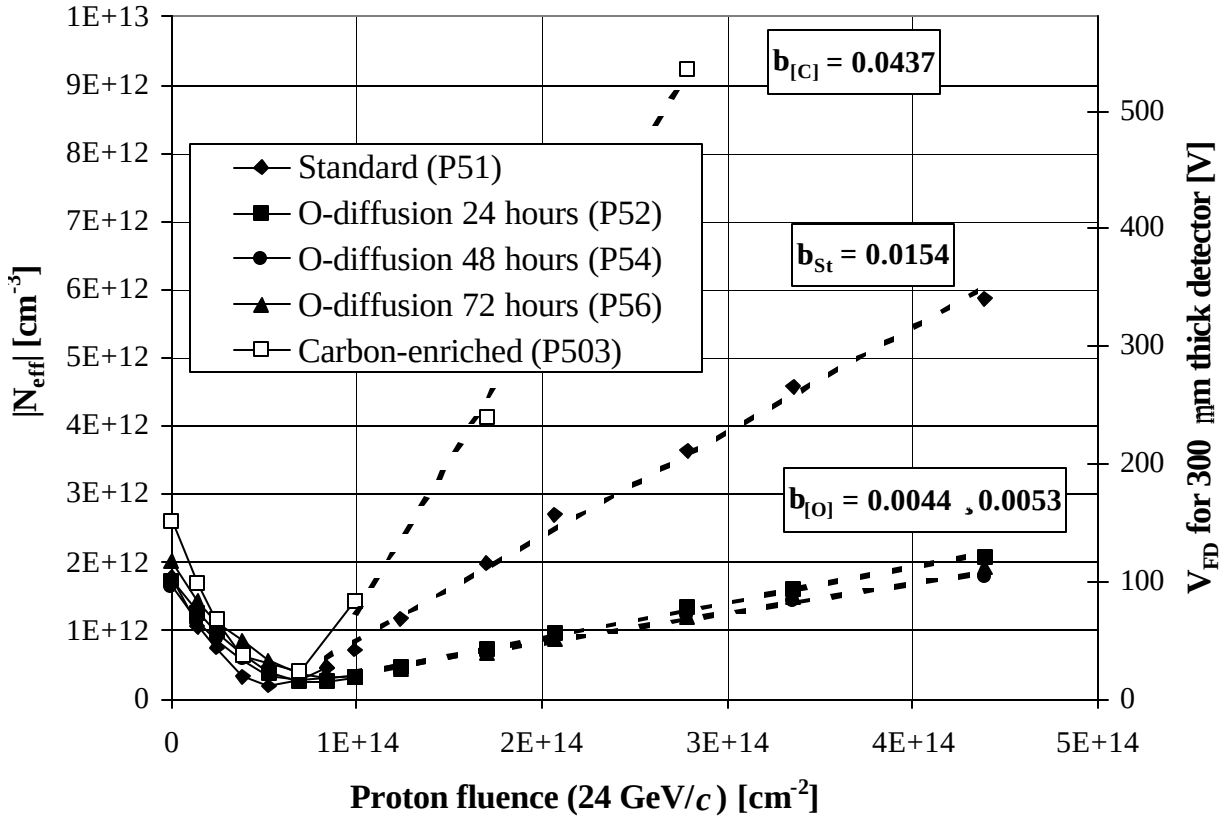

Figure 10: Effective space charge density and full depletion voltage versus proton fluence for standard, carbon-enriched and three types of oxygen diffused samples: 24, 48 and 72 hour diffusion at 1150°C [17].

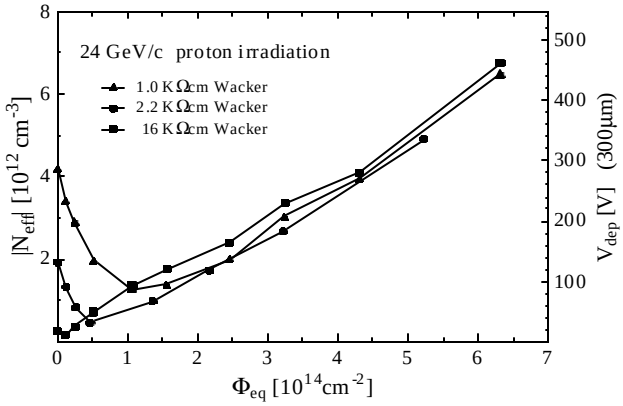

Fig. 11.: 24 GeV/c proton irradiation of O-rich diodes with different resistivity.

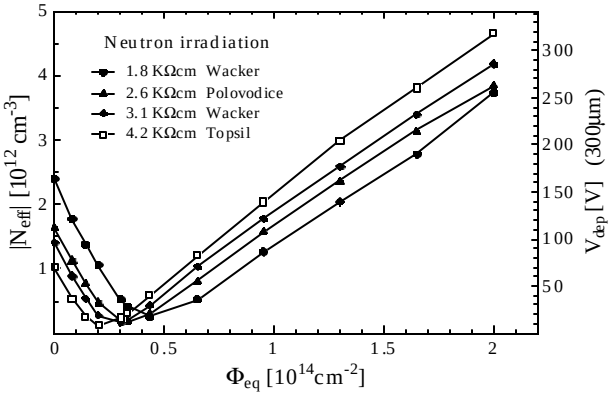

Fig.12: Reactor neutron irradiation of O-rich diodes with different resistivity.

Full annealing cycles and complete modelling

As stated above, the CERN-scenario measurements have proven to be extremely useful for a fast damage evaluation of different material. Only this way was it possible to select the most promising defect engineering process resulting in an appreciable improvement of radiation hardness. However these measurements allow one to measure only one of the relevant parameters, namely the effective doping concentration at or around the minimum of the annealing function. A different approach, introduced by the Hamburg group [18], uses a set of diodes processed from the same material and individually irradiated by different fluences. Each diode then undergoes a full annealing cycle. This is a time consuming effort but allows the study of all components in the change of the effective doping concentration in the most systematic way. An example of the whole complex behaviour is given in Fig.13. ΔN_{eff} is the damage induced change in the effective doping concentration with respect to its initial value before irradiation.

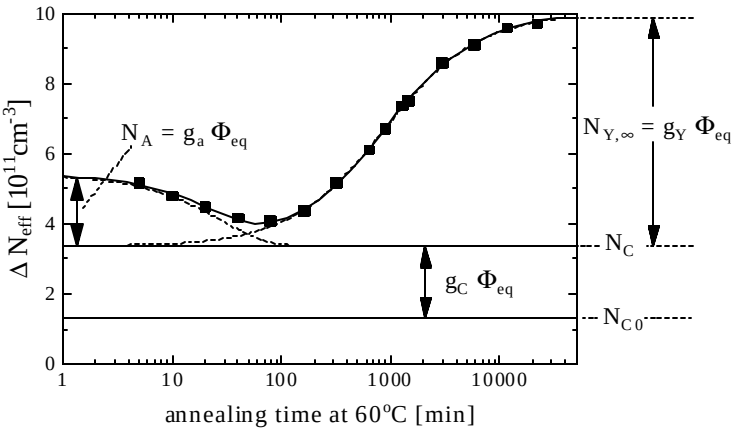

Fig.13: Annealing behaviour of the radiation induced change in the effective doping concentration ΔN_{eff} at 60°C.

$$\Delta N_{eff}\left(\Phi_{eq}, t(T_a)\right) = N_{eff,0} - N_{eff}\left(\Phi_{eq}, t(T_a)\right) \quad (6)$$

As function of time and fluence ΔN_{eff} can be described as:

$$\Delta N_{eff}\left(\Phi_{eq}, t(T_a)\right) = N_A\left(\Phi_{eq}, t(T_a)\right) + N_C\left(\Phi_{eq}\right) + N_Y\left(\Phi_{eq}, t(T_a)\right) \quad (7)$$

In this equation it has been explicitly denoted that the time dependence is in itself subject to the annealing temperature T_a. As indicated in Fig.13 and obvious from eq.(7) ΔN_{eff} consists of three components, a short term beneficial annealing N_A, a stable damage part N_C and the reverse annealing component N_Y. N_C can be described by an incomplete donor removal, depending exponentially on the fluence with a final value N_{C0} and a fluence proportional introduction of stable acceptors with an introduction rate g_C:

$$(8) \qquad N_C(\Phi_{eq}) = N_{C0}\left(1-\exp\left(-c\Phi_{eq}\right)\right) + g_C\Phi_{eq}$$

As can be seen from Fig.13, disregarding the still present component from the beneficial annealing and a starting reverse annealing part, N_C should obey a very similar dependence on Φ_{eq} as exhibited in the CERN scenario experiments and hence there is a close relation between β of those measurements and the introduction rate g_C given here. Finally the reverse annealing component appears to be best described by a 2nd order process with amplitude $N_Y = g_Y \Phi_{eq}$ and a dependence on the annealing time according to $[1-1/(1 + t/\tau_Y)]$. It should be noted that this function is quite identical to a 1st order approach according to $[1 - exp(-t/\tau_Y)]$ for moderately short annealing times but differs appreciably in approaching the saturation value. It has also been shown that the temperature dependence of the time constants involved in the annealing processes are strictly governed by activation energies and having measured these values one can easily transfer the annealing function obtained at high temperature (for the sake of acceleration of the measurement) to any given value. With respect to a room temperature measurement this acceleration factor for the reverse annealing is e.g. 550 for a 60°C and 7400 for an annealing at 80 °C.

How well this model describes the real data obtained for a large set of different fluences and annealing times spanning 3 orders of magnitude, may be demonstrated in Fig.14. Each full line is the result of a fit employing the functional dependence as described above. Using such evaluations the different damage parameters, i.e. N_A, τ_A, N_C, N_Y and τ_Y can be derived.

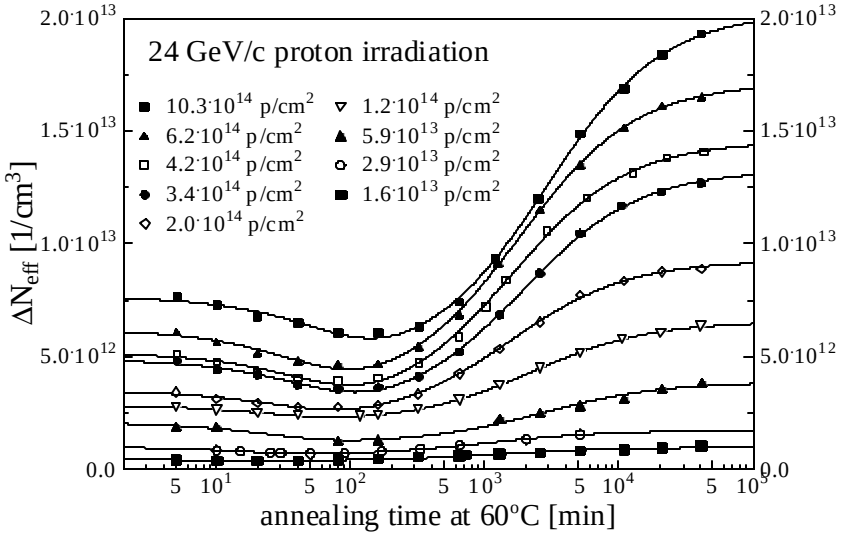

Fig. 14: Annealing of oxygen enriched diodes at 60°C after irradiation with 24 GeV/c protons

The results of such analysis for neutron irradiated Oxygen enriched diodes are given in Fig.15 for the beneficial annealing, Fig.16 for the stable damage component and Fig.17 for the reverse annealing. As stated above the introduction rate for stable acceptors g_C, analysed this way and found to be $2\ 10^{-2}\ cm^{-2}$ (Fig.16) is indeed very close to the *β-value* measured in the CERN scenario experiment of Fig.13. The nice fluence proportionality of the amplitudes for the beneficial and reverse annealing and their independ-

ence of the annealing temperature as seen in Fig.15 and Fig.17 plus the good fit in Fig.16 according to eq.(8) are certainly a convincing demonstration of the quality of the model description.

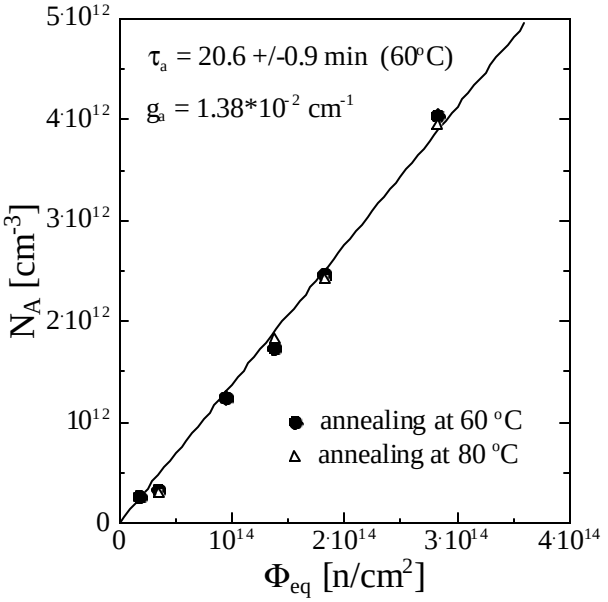

Fig.15: Beneficial annealing N_A for neutron irradiated oxygen enriched silicon.

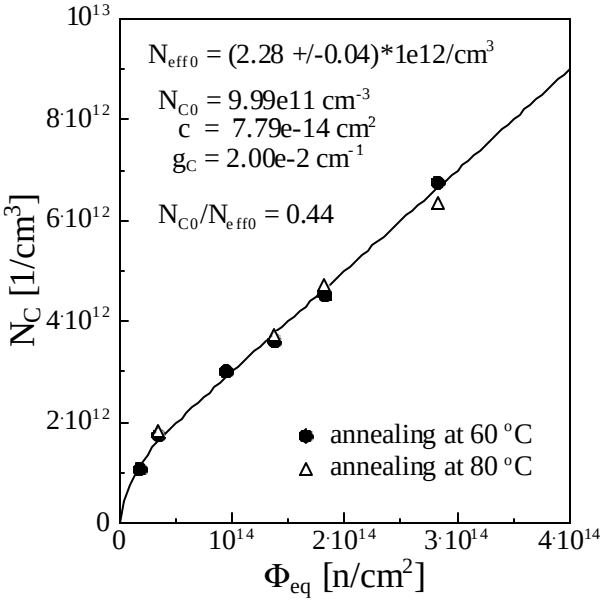

Fig.16: Stable Damage component N_C for neutron irradiated oxygen enriched silicon.

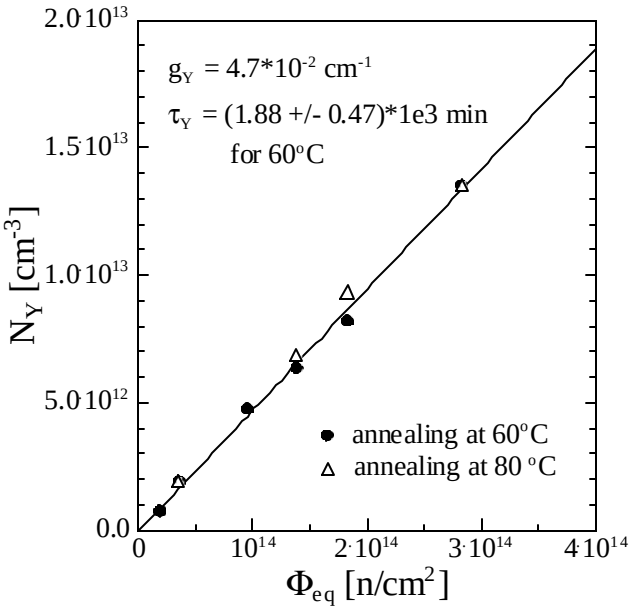

Fig.17: Reverse Annealing N_Y for neutron irradiated oxygen enriched silicon

In Figs.18 to 20 the proton damage results for Oxygen enriched diodes are given and compared to those obtained with standard material. Again, as was clear already from the *b-values* extracted from the CERN scenario measurements (Fig.10), we see a very pronounced improvement in the introduction rate of stable acceptors. With respect to standard material the oxygen enriched silicon is radiation harder by a factor of $g_C(standard)/g_C(oxygen.) = 3.5$ (Fig.18). In addition we have observed the really surprising effect, that in contrast to standard silicon, the reverse annealing amplitude is not proportional to the fluence anymore in oxygenated silicon but shows a significant saturation effect, as shown in Fig.19. In fact due to the steep increase of that amplitude for standard material the largest fluence for which the full annealing cycle could be measured was $F_{eq}=3.5\ 10^{14}$ cm^{-2} whereas the Oxygenated silicon measurements could be extended to almost double that value. The observed reduction in N_Y is at least a factor of 2, and would even increase at larger fluence. It was likewise surprising that in addition to this effect, the time constant for the reverse annealing process is increasing, and depends on the Oxygen concentration. It shows an improvement by a factor of 4 with respect to standard diodes (Fig.20). Both these effects, the reduction of the reverse annealing amplitude and the much longer time period before the final value will be reached are regarded to be extremely important for the LHC applications. As the reverse annealing is mainly encountered during the warm up periods necessary every year, this behaviour offers a much welcome safety margin for operation.

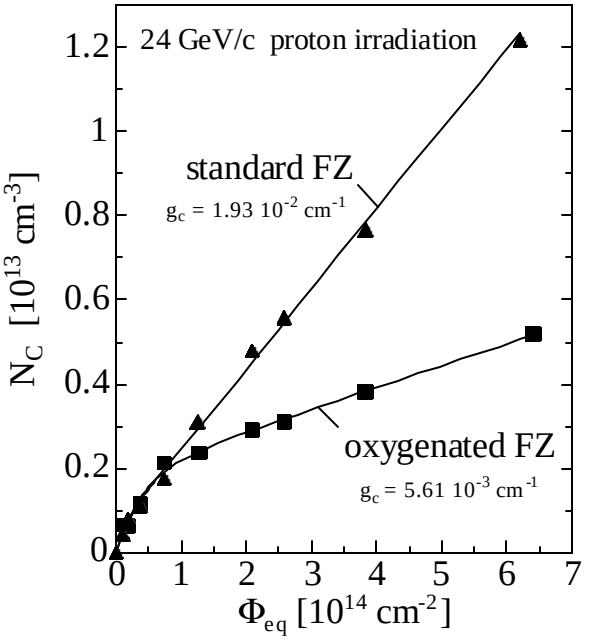

Fig.18: Damage parameters N_C for oxygenated and standard material as obtained from annealing experiments at 60°C after irradiation with 24 GeV/c protons.

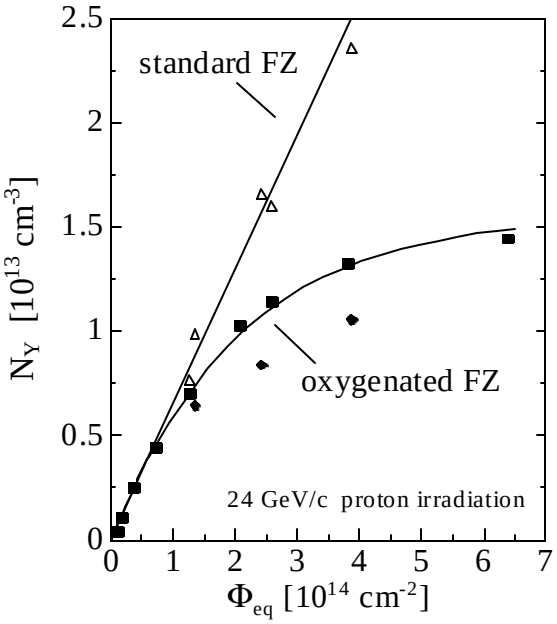

Fig.19: Damage parameters N_Y for oxygenated and standard material as obtained from annealing experiments at 60°C after irradiation with 24 GeV/c protons.

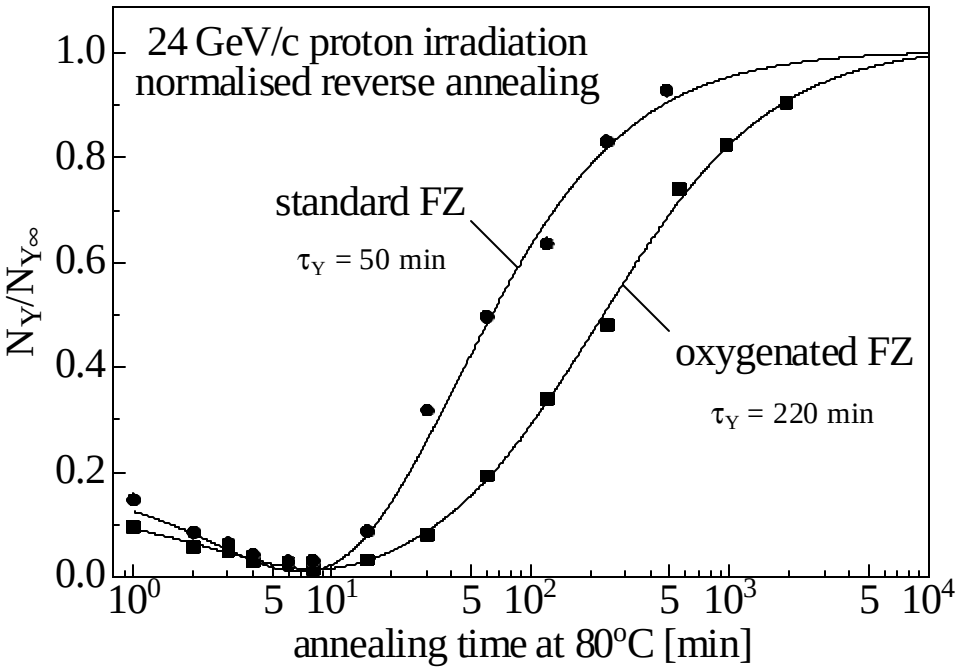

Fig.20: Reverse annealing for standard and oxygen enriched diodes after irradiation with 24 GeV/c protons (Φ_{eq} = 2 10^{14}cm^{-2}). The time constant is increased for oxygen enriched diodes.

Charge collection measurements

The LHC experiments are naturally less concerned with the depletion voltage measured by normal C/V techniques which gives the effective doping concentration but concentrate on the operating voltage needed to guarantee a good S/N ratio for the detection of mip's. Hence the prime objective is to assure a given charge collection efficiency. Due to trapping and other effects, the bias voltage needed for this might in fact be appreciably larger than the depletion voltage deduced from C/V measurements or from the model. A

proper comparison between results obtained from the C/V method and those extracted directly from charge collection measurements is therefore required. Such experiments can be performed with a beta-source which provides real minimum ionising particles or using a long wavelength IR-laser light with an ultrashort pulse duration. The laser source simulates a mip like ionisation in the diode. Both techniques are extremely time consuming in contrast to the C/V-method. Hence they have so far only been performed on selected samples as a consistency check. Fig. 21 gives an example for a real ATLAS prototype strip detectors processed by MICRON irradiated with 3 10^{14} p/cm^2 (the standard ATLAS test fluence) and annealed at 80°C for 4 minutes [19].

The following two results are evident: The oxygenated detector shows an improved charge collection as function of bias. 85% of the full charge collection, as measured with the Ru-beta-source is already reached at 150 V whereas 225 V are needed for the non oxygenated one. This is in quite good agreement with expectations from C/V measurements. In addition, the measurements performed with the Ru-source agree very well with those using the pulsed laser, which are much easier to perform. Fig.22a and b show examples for two different test diodes (oxygenated and standard) irradiated with 4 and 8 10^{14} p/cm^2 respectively and annealed at 80°C for 4 minutes. The agreement between the charge collection results and those obtained by C/V measurements are quite satisfactory. As a matter of fact the bias voltage needed for 85% charge collection efficiency is in both examples very close to the depletion voltage, the remaining 15% of the signal height is attributed to trapping. A complementary presentation of these results is shown in Fig.23, where the charge collection inefficiency is plotted versus the inverse bias voltage for values above the depletion voltage. It nicely demonstrates that test diodes and strip detectors behave almost identically while there is a substantial improvement to be seen for oxygenated silicon against the use of standard material. Another example of comparison between the results obtained from C/V measurements and those from charge collection is shown in Fig.24. Here the test diodes have been completely annealed after irradiation. In this case the illumination is made from the p^+-side with a short wavelength laser of only 670 nm. The carriers are generated in a very shallow layer of only a few microns due to the very short absorption length of this light. As the material is type inverted at these fluences, the electric field starts to grow from the rear side and reaches the p^+-electrode only at full depletion. Hence measuring the charge collection as function of bias provides a very sensitive tool for the measurement of the depletion voltage. The almost complete agreement between the two measurements supports the results for the saturation of the reverse annealing displayed in Fig.19 very nicely. The N_{eff}*-values* extracted from the data of Fig.24 suggests an even larger saturation effect than that shown in Fig.19.

Finally measurements on charge collection using an oxygenated detector have been performed in a strong magnetic field [20]. Examples of these results are presented in Fig. 25. Also in this case a short wavelength IR-laser (λ = 850nm) ensuring a shallow absorption was used and the diode was illuminated from the p^+ side for measurement of the electron contribution and from the rear one for the holes. The full depletion voltage after 7 10^{13} p/cm^2 was of the order of 100 V and the material was type inverted. As the holes are thus generated in an area of high electric field and the electrons at low field strength, the difference in their behaviour as function of bias voltage is understandable. It is reassuring that the reduction in signal height observed due to a magnetic field of 4T is not appreciable. This effect is a consequence of the Lorentz angle resulting in larger drift lengths and hence increased trapping.

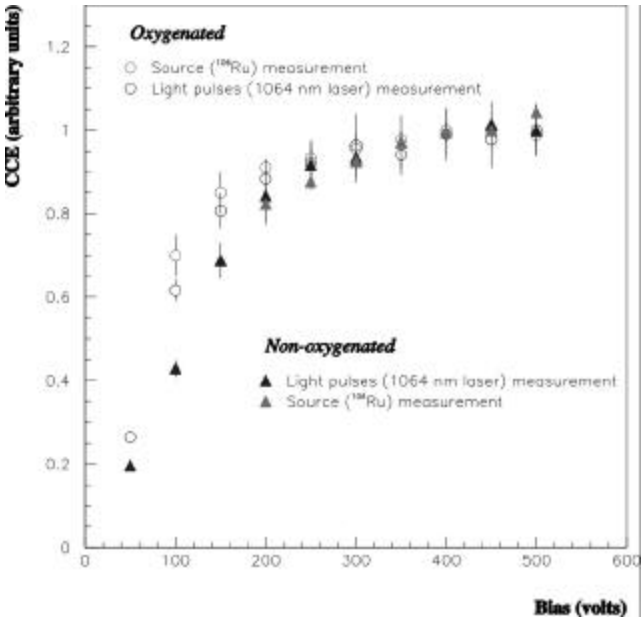

Fig. 21 CCE of ATLAS prototype strip detectors processed by MICRON and irradiated with 3 10^{14} p/cm^2 [19].

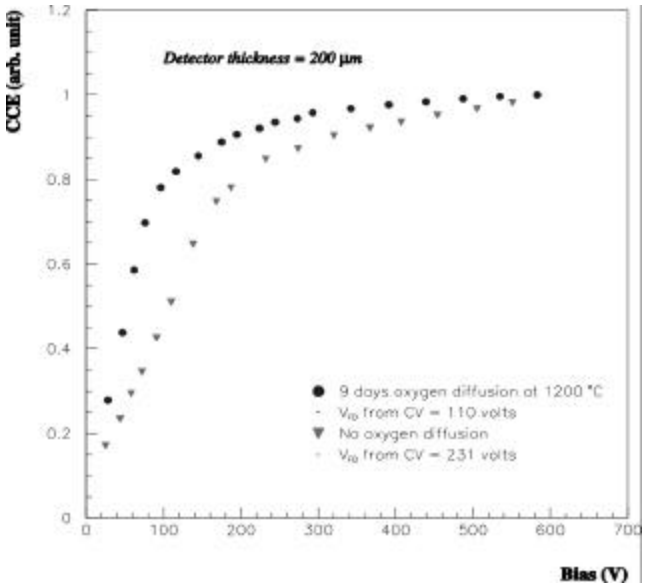

Fig.22b: CCE (1060 nm laser) of standard and oxygenated diodes irradiated with 8 10^{14} p/cm^2 [19].

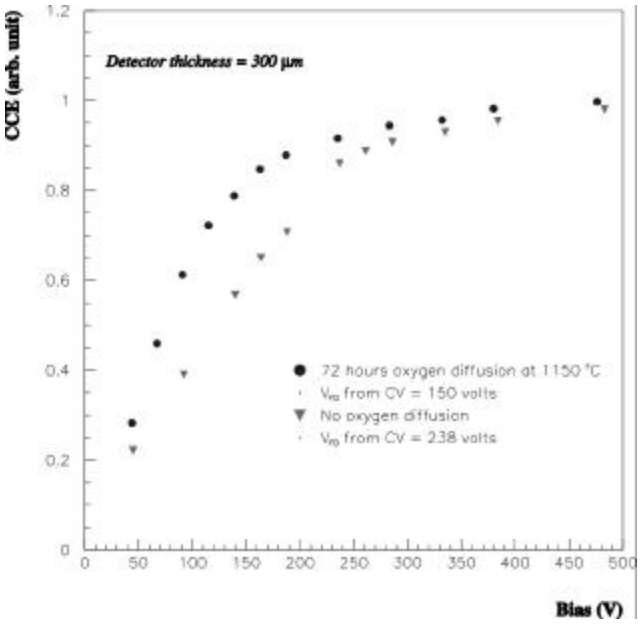

Fig.22a: CCE (1060 nm laser) of standard and oxygenated diodes irradiated with 4 10^{14} p/cm^2 [19].

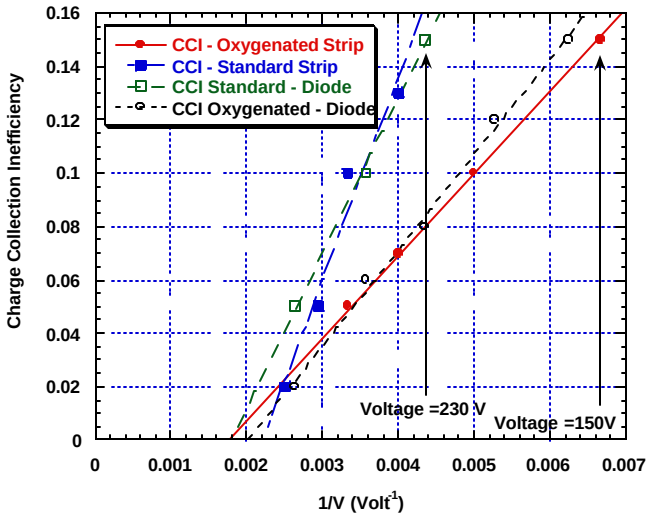

Fig.23: Charge collection inefficiency as function of bias voltage above full depletion. Data from Figs. 21 and 22a.

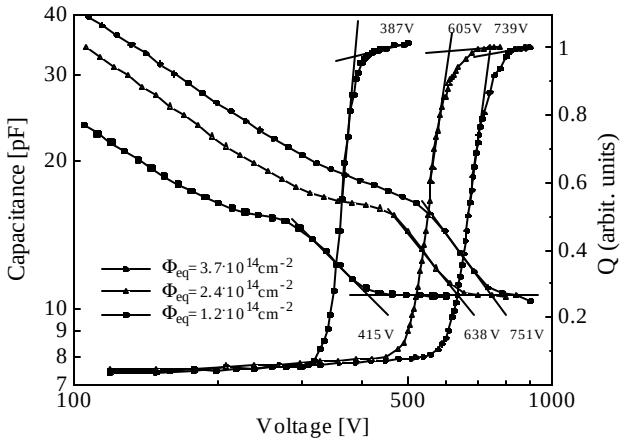

Fig.24: 24 GeV/c proton irradiated oxygenated silicon detectors (2, 4 and 6×10^{14} p/cm^2). Comparison of depletion voltages determined by CV (10 kHz) and TCT (front illumination, 670nm, 40ns integration).

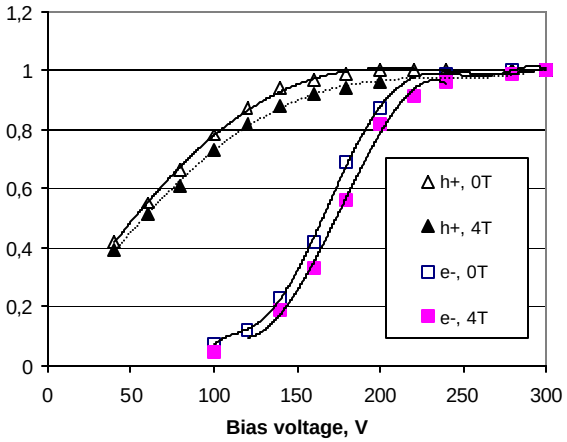

Fig.25: CCE (850 nm laser, 25ns integration) of proton irradiated oxygenated diodes with and without magnetic field [20].

Table 2.: Damage parameters for oxygen enriched and standard silicon.

	Standard Silicon		Oxygen-enriched Silicon	
	Neutrons	Protons	Neutrons	Protons
g_a	1.8×10^{-2} cm^{-1}	-	1.4×10^{-2} cm^{-1}	-
$\tau_a(20°C)$	55 h	-	70 h	-
g_C	1.5×10^{-2} cm^{-1}	1.9×10^{-2} cm^{-1}	2.0×10^{-2} cm^{-1}	5.3×10^{-3} cm^{-1}
N_{C0}/N_{eff0}	0.70	-	0.45	1.0
g_Y	5.2×10^{-2} cm^{-1}	6.6×10^{-2} cm^{-1}	4.8×10^{-2} cm^{-1}	2.3×10^{-2} cm^{-1} (♣)
$\tau_Y(20°C)$	480 d	-	800 d	950 d

(♣) saturation value measured for $\Phi_{eq} = 6\ 10^{14}$cm^{-2}

Parameters of the Hamburg model and application to the LHC

Once a set of reliable parameters has been extracted from the various damage test experiments it is then possible to apply the model description outlined above to the operational scenario of the LHC experiments. It should be emphasised here that the conservative values listed in Table 2 are still subject to some uncertainties. In contrast to the behaviour of the current related damage parameter α, which has been shown to be completely independent of material properties and different processing techniques, variations for the parameters describing the change of the effective impurity concentration are in the order of 50%. They are certainly much smaller than the really outstanding improvements observed with Oxygenated silicon in comparison to standard material. The main results using O-rich material in comparison to standard silicon are:

Proton irradiation

- The introduction rate for stable acceptors g_C is a factor of 3.5 lower.
- The reverse annealing effect is considerably reduced both due to a saturation at high fluences (resulting in at least a factor of 2) and the much longer time constant (by a factor of 4).
- There is no effect from the initial resistivity of the material (due to complete donor removal)
- The results obtained with C/V measurements have been nicely reproduced with those obtained from charge collection.

Neutron irradiation

- The introduction rate for stable acceptors appears to be the same as for standard silicon.
- The reverse annealing is not affected by Oxygenation.
- There is an appreciable beneficial effect using O-rich low resistivity silicon

It should be noted that operational projections for the behaviour of the silicon detectors to be incorporated in both the ATLAS, CMS and LHCb have already been carried out on the basis of the Hamburg model. An update using the new parameters obtained for the Oxygenated silicon detectors is shown in Fig. 26a and b. As an example, the two pixel layers of the ATLAS detector are chosen, where the pion irradiation is most severe. The ATLAS B-layer is subject to a total fluence of $F_{eq} = 3\ 10^{15}\ cm^{-2}$ accumulated within 10 years of LHC operation. Simulation results are shown in Fig.26a. Here the pixel-detectors have a thickness of *200mm* and will be operated at a maximum bias voltage of *600 V*. The depletion voltage will reach this limit already after 4 years of operation, using standard silicon detectors, whilst the application of Oxygen enriched silicon would extend that time to 6 years. However, the ATLAS pixel group envisages to operate the detectors in partially depleted mode, requiring only a signal height of *6000 e/mip*. Using this reduced requirement the operational lifetime for standard silicon would be extended to *6 years* while Oxygen enriched detectors could be almost operated for the full *10 year* period!

In Fig.26b we display the results for the 1st layer at *10 cm* again in the ATLAS pixel subdetector. Here the calculations have included the mixed field (approximately 70% pions, 30% neutrons), which account for a total fluence of $Feq = 7\ 10^{14}\ cm^{-2}$. In this case the detectors will have a thickness of *250mm* and total depletion is required at a maximum voltage of *600V*. This limit is reached after *8 years* for standard silicon while Oxygen rich silicon is easily operable during the full LHC period. From both examples it is obvious that the use of the radiation hardening process offered by the RD48 results, provides an appreciable improvement for safe operation of silicon detectors in the inner detectors of the large LHC experiments. It should also be emphasised at this point that the operational scenario for e.g. the ATLAS detector requires a warm up period of only 2 weeks every year. The results of Fig.26a and b were based on the assumption that this requirement can really be fulfilled during 10 years! As longer warm up periods or accidents would result in a much larger contribution from the reverse annealing effect, the appreciable improvements obtained by Oxygenated silicon in this respect (see above) provide an additional invaluable safety margin.

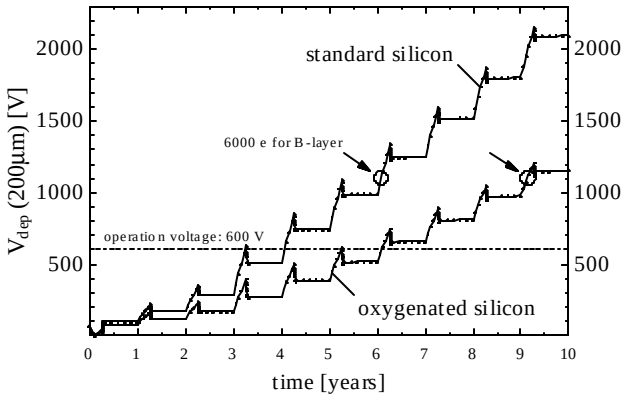

Fig.26a.: Damage projection for the ATLAS B-layer demonstrating the difference between standard and oxygenated silicon.

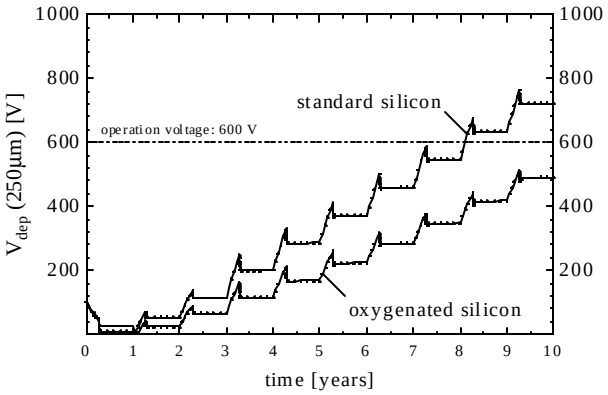

Fig.26b.: Damage projection for the ATLAS 1st-layer demonstrating the difference between standard and oxygenated silicon.

5. EFFECTS AT THE Si/SiO_2 INTERFACE

In addition to standard test diodes intended for investigations of bulk damage effects, a set of gate-controlled diodes were included in the ROSE mask layout [21]. These structures are perfectly suited to the analysis of the oxide quality, as both oxide charge and the e-h pair generation process at the interface can be determined independently. Ionising radiation is know to lead to an increasing oxide charge and interface state density, which results in corresponding changes in the depletion depth and the leakage current of strip detectors. The as-processed quality of the interface as well as its sensitivity to radiation are strongly dependent on the details of the device processing. It is therefore very important to doublecheck, how the use of oxygen-enriched and lower resistivity material affect the interface properties.

Fig. 27 displays two measurements of the interface generation current on oxygen-enriched samples processed with different processing parameters. The interface generation current is equal to the height of the current step at the flat-band voltage of about 2.5 V. Comparing the values with non-oxygenated silicon, a similar interface quality is found for the as-processed devices.

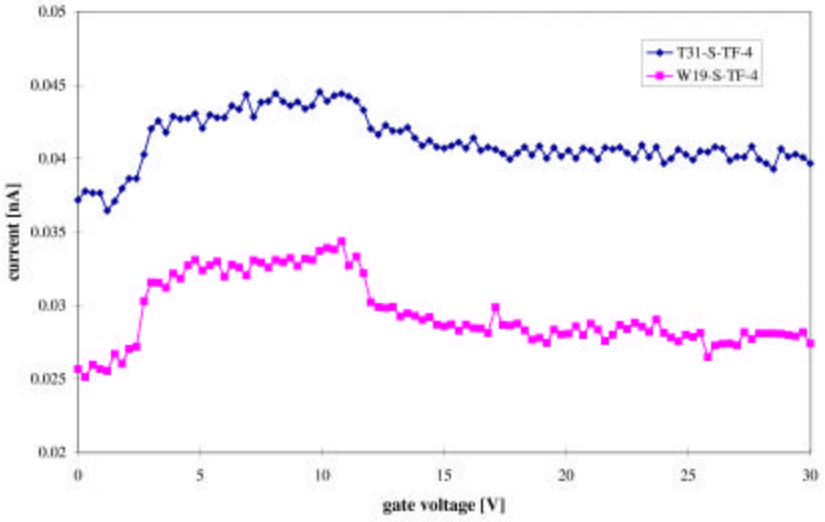

Fig. 27. Measurements of the interface generation current for two differently processed gate-controlled diodes manufactured on oxygen-enriched material.

The relatively low flat-band voltage indicates a high-quality oxide. After exposing the oxides to electrons from a Scanning Electron Microscope, the density of positive trapped oxide charges increased, which is manifested by the shift of the flat-band voltage, see Fig. 28. The curves differ according to the different oxide thickness, but the oxide charge density is similar for both devices, and as expected its value is about 3×10^{12} cm^{-2}. The results of the study are summarised in Table 3.

Table 3. Results of the study on the radiation sensitivity of the oxides grown on oxygen-enriched silicon.

Device	**N_{ox} [$10^{11}/cm^2$]**	**D_{it} [$10^{10}/cm^2eV$]**	**Dose [kGy]**
W19-S-TF-4	0.6	0.7	0
T31-S-TF-4	0.6	0.7	0
W19-S-TF-4	21	30	200
T31-S-TF-4	35	30	200

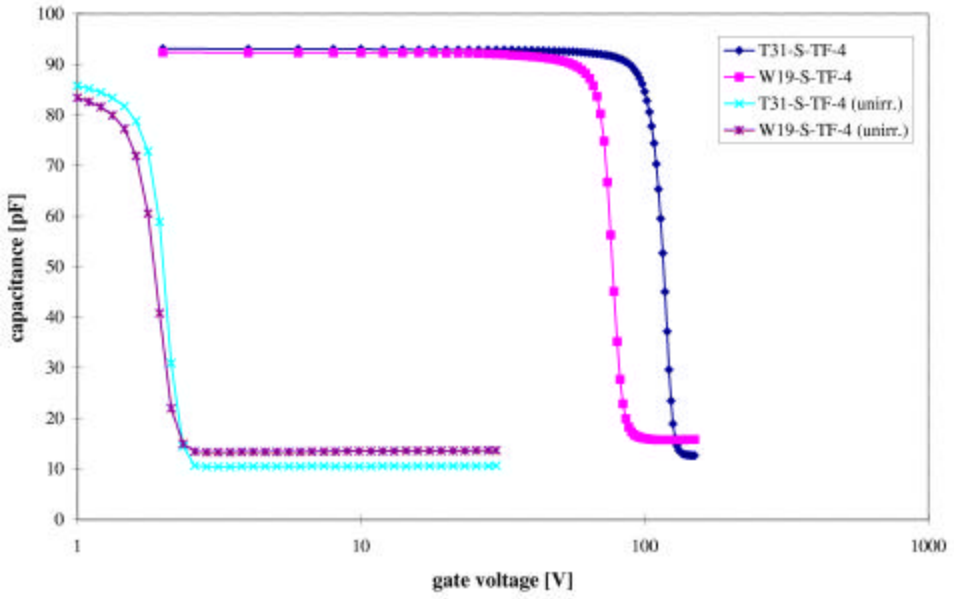

Fig. 28. Capacitance-voltage characteristics on the gate electrode of the gate-controlled diodes before and after exposure to ionising radiation.

6. DEFECT SPECTROSCOPY

Along with the phenomenological studies on the damage-induced deterioration of the detectors, defect spectroscopy has always been carried out within the collaboration. A detailed knowledge about the microscopic origin of the changes in leakage current, effective doping concentration, and carrier trapping is inevitably needed as the groundwork for the defect-engineering approach: Detrimental defects must be structurally and chemically identified before wise choices can be made regarding the optimisation of the impurity content of the silicon in order to suppress the defect's production following irradiation. In fact, the decision in favour of oxygen-enriched, carbon-lean, lower resistivity material is to a large extent motivated by the known interactions between the primary displacement damage defects (interstitials and vacancies) with the most prominent impurities (Oxygen, Carbon, Phosphorus, Boron), well reported in literature for more than a decade. Using this heuristic approach, more radiation tolerant silicon has been successfully engineered by the collaboration even though there is much still to learn about the microscopic processes leading to the deterioration of silicon detectors. Much time consuming work has been carried out in order to discover previously unreported defects, to account for the peculiarities of heavy-particle damage, and to handle the experimentally difficult high-resistivity material. As will be shown below, many significant new results have been obtained in this field.

The following section is organised into three parts. In the first part the main spectroscopic tools available within the collaboration are briefly introduced, highlighting the kind of information that can be gained with them and indicating experimental requirements for their application. The second part discusses results obtained after irradiation with various particle types and using different materials, and the third part reviews examples where spectroscopic signals could indeed be unambiguously related to a certain macroscopic quantity.

Damage-Induced Defects as Observed with Various Spectroscopic Characterisation Tools

Capacitance-Deep Level Transient Spectroscopy (C-DLTS)
In C-DLTS the capacitance of a reverse-biased diode is used as a probe of the charges in the space charge region. The charges are the doping atoms and defects that were allowed to trap free carriers during a preceding filling pulse. Following the pulse, the capacitance approaches its steady state value exponentially with a time constant characteristic for the emission of carriers from the traps into the band. The DLTS signal is derived from this transient, e.g., using the difference of the capacitance at two different times (boxcar). Plotting the DLTS signal versus temperature gives a spectrum with a peak for each level in the band gap of the semiconductor, see Fig. 29.

Good C-DLTS set-ups provide the emission-parameters (activation energy ΔE and cross section σ) and the concentrations N_t of all traps within one temperature scan. Traps throughout the entire band gap, except for very shallow levels, can be detected, and majority and minority carrier traps can be distinguished. With some extra effort, the free carrier trapping kinetics (capture coefficients) can be studied. While the trap concentrations derived from DLTS measurements are the most accurate values available compared with all other tools discussed below, C-DLTS is strictly limited to trap concentrations well below the doping concentration. For the high-resistivity material studied here this means that the fluence must be very low, orders of magnitude lower than is anticipated during the operation of the detectors.

In Fig. 29 we observe all well-known signals from damage-induced defects in silicon and the corresponding isochronal annealing behaviour. Evidently Oxygen and Carbon play an important role as sinks for the primary damage defects (interstitials and vacancies). In fact, the ratio between the C_iC_s and C_iO_i signals in conjunction with their annealing rate can be exploited to determine both the O and C concentration. The more relevant observations for today's discussion concern the less abundant and unidentified peaks (e.g. E_V + 0.312 eV), the left and right-hand side broadening of the $VV^{-/0}$ transition, and/or the apparent concentration difference between the doubly charged and singly charged divacancy peak observed before the 280°C annealing step. The two latter observations are currently discussed within the framework of the defect cluster strain model and the inter-centre charge transfer model described in refs. [22] and [23], respectively.

Thermally Stimulated Current (TSC)
In order to obtain a TSC spectrum, the defect filling pulse is applied only once at low temperature, and the TSC signal is simply given by the leakage current through the reverse-biased detector during the heating period, see Fig. 30. While TSC was originally used analogous to DLTS, it was realised in this collaboration that a TSC signal can still be measured even if the trap concentrations are higher than the doping concentration, if forward current injection or optical injection of free carriers is used for the trap filling. However, in this case it is not straight-forward to distinguish between majority and minority carrier traps or to determine trap concentrations. Also, measuring ΔE and σ requires much more experimental effort as compared to DLTS. Traps throughout the entire band gap are observed, including very shallow traps (e.g. the Phosphorus donor level). However, signals from deep traps are often hidden below the steady state leakage current of the device, which constitutes the baseline signal of the method.

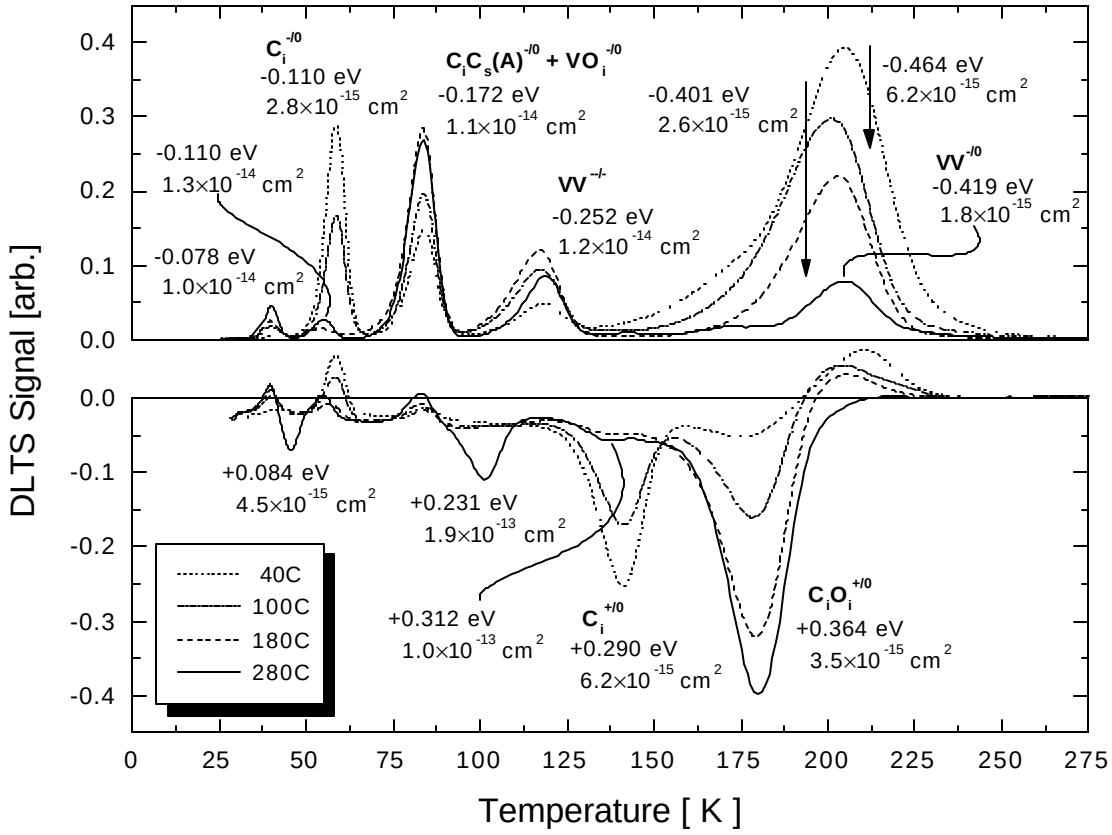

Fig. 29. Isochronal annealing (ΔT = 20°C, Δt = 20 min) of DLTS spectra after radiation damage with 10^{11} <5.3 MeV> neutrons per cm^2 (3 kΩcm n-type epitaxial material) [24].

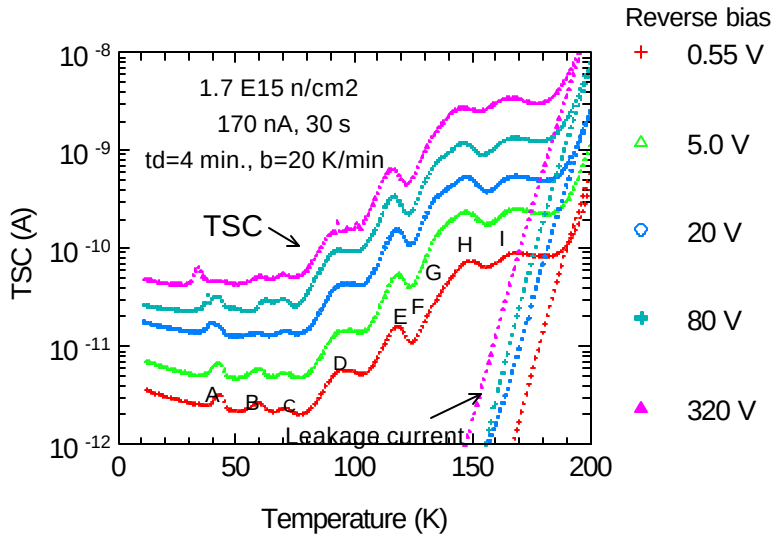

Fig. 30. Reverse-bias dependence of TSC spectra [25].

Current-DLTS (I-DLTS) and Photo-Induced Current Transient Spectroscopy (PICTS)

In order to combine the higher sensitivity and faster access to ΔE and σ provided by C-DLTS with the ability to measure trap-compensated high-resistivity material, the detector leakage current can be used as the signal for the DLTS method. This approach is known as I-DLTS and/or PICTS, where the latter represents an effort to determine trap concentrations from photo-induced current transients exploiting addi-

tional experimental information. Also I-DLTS is commonly used in combination with optical excitation. Rather detailed spectra can be obtained, see Fig. 31, but the status of trap assignment is not as advanced as compared to C-DLTS.

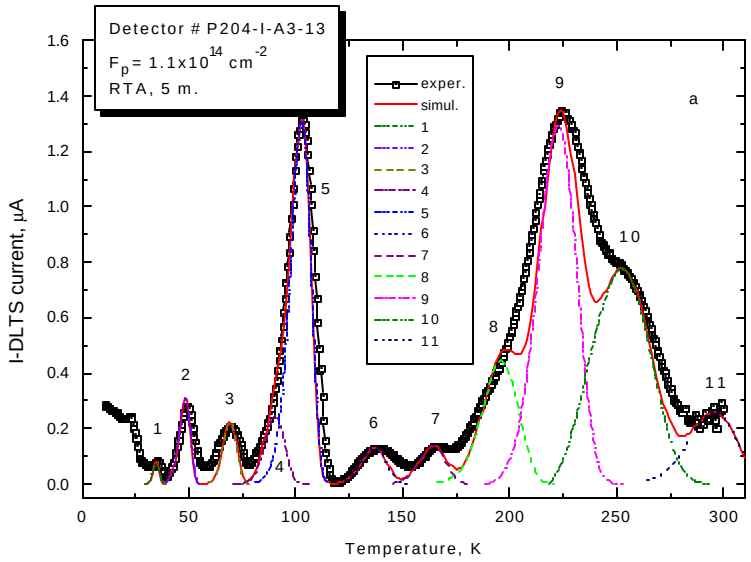

Fig. 31. Experimental I-DLTS spectra of silicon detectors irradiated to a high fluence, and the corresponding simulated spectra. Dashed/dotted lines show the components of the simulated spectra [26].

Optical Charging Spectroscopy (OCS)

OCS is a method related to TSC. Traps are filled at low temperature using illumination with light of various wavelengths to modulate the depth profile. The short-circuit current is measured during warm-up. See Fig. 32 for a comparison between TSC and OCS. This method is sensitive to traps close to the junction of the diode.

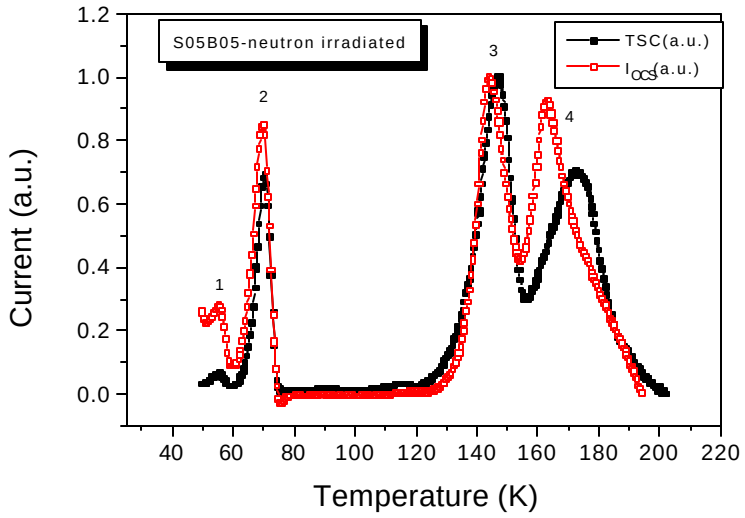

Fig. 32. TSC (V_{up} = 150 V) and OCS (V_{up} = 0 V) currents (arb. units), $\Phi_{eq} = 1.8\times10^{13}$ n/cm^2 [27].

Transient Current Technique (TCT)

Here free carriers are generated with a short (1 ns) laser pulse below either front or backside of the detector. The signal is given by the current induced by the drifting carriers. At low temperatures the free carriers can also be trapped at defects, which modulates the electric field in the detector and thus affects the pulse shape, compare Fig. 33. Studying the signal as function of temperature gives spectroscopic information about the traps. TCT is applicable for medium radiation fluence (about 10^{13} cm^{-2}), where the electric field in the fully depleted detector is so low that the drift time of the carriers is well above the resolution of about 1 ns. TCT is a complementary method as it is very sensitive to traps close to the middle of the band gap. For example, a deep hole trap at E_V + 0.5 eV has commonly been observed, which might be very important for the generation of leakage current [28,29].

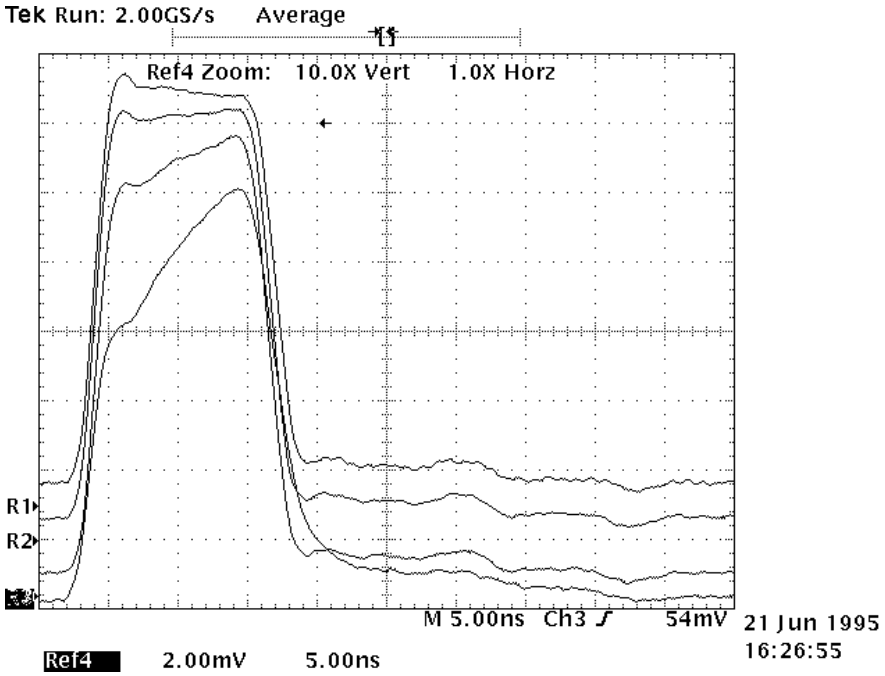

Fig. 33. Measured steady-state electron current pulse shapes at various temperatures for an irradiated detector R1: 170K; R2: 165K; R3: 160K; R4: 155K (4 kΩcm, d = 630 μm, V = 100V, $\Phi_n = 2.3\times10^{12}$ cm^{-2}, 31 months room temperature) [28].

Photo Luminescence (PL)

PL is an optical method, and does not require electrical contacts to the sample. Electron-hole pairs are excited in the material with above band-gap light. At low temperature the electron and hole form a weakly bonded pair, which can diffuse through the crystal as an entity. This so-called exciton can get trapped at a defect, where it eventually will recombine and thus cause the emission of a photon characteristic of the defect. Fig. 34 shows a typical PL spectrum as observe on standard float-zone material after proton irradiation. Note that besides the known C_iC_s and C_iO_i signals the mysterious W-line is observed. Recent quantum mechanical modelling indicates that the W-line may be the tri-interstitial. Optical selection rules and oscillator strengths determine whether a deep level defect gives rise to a PL signal and how strong it is. It is therefore not in general possible to obtain concentrations from PL measurements; many defects cannot be detected at all, e.g. VO_i. PL is very sensitive (10^{10} cm^{-3}) given the number of nonradiative recombination centres is sufficiently small.

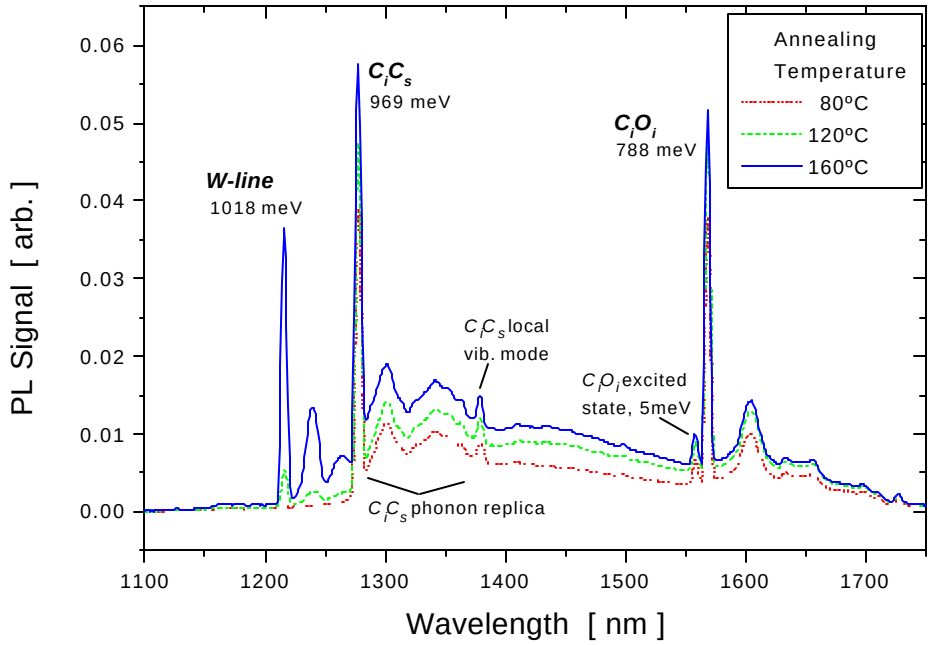

Fig. 34. Annealing of Photoluminescence spectra measured on heavy-particle damaged silicon [30].

Results for Different Particle Types and Materials

In the following we will present systematic studies on the influence of the particle type used for irradiation and of the impurity content of the material. In part, these experiments were designed to elucidate the circumstances leading to the improved radiation tolerance of oxygen-enriched silicon only observed for charged-particle irradiation.

Gammas Versus Neutrons

A direct comparison of the radiation defects produced by ^{60}Co-γ and 14 MeV neutrons has been carried out on 3 kΩcm standard Wacker FZ material, see Fig. 35 [14]. With gammas, only randomly distributed point defects are produced, whereas neutrons give rise to damage cascades and end-of-range damage. The samples were maintained at room temperature for a few months before the measurements. While for the gamma-irradiated sample the ratio [VV(-/0)]/[VV(=/-)] between the apparent concentration of the two divacancy-related peaks is found to be 1.0, the neutron-irradiated sample displays a 3.3 times weaker signal from the doubly-to-singly charged transition. This discrepancy was discovered earlier by Svensson et al. and was explained by lattice strain effects, which then also would account for the peak broadening [22]. The strain arises from divacancies being predominantly produced within each others lattice strain field at the end of range of the recoil cascades. Another explanation was put forward by S. Watts et al., realising that such closely spaced defects might as well be able to exchange electrical charges [23]. This is the so-called inter-centre charge transfer model also explains the suppression of the VV(=/-) signal.

Divacancies are produced in much larger amounts in neutron-damaged samples as compared to gammas. The corresponding ratios between the introduction rates $g = N_t/\Phi$ found in this study are:
gammas: $g(VV^{-/0})/g(VO_i) = 0.029$, and neutrons: $g(E(205))/g(VO_i) = 1.49/0.69 = 2.15$.

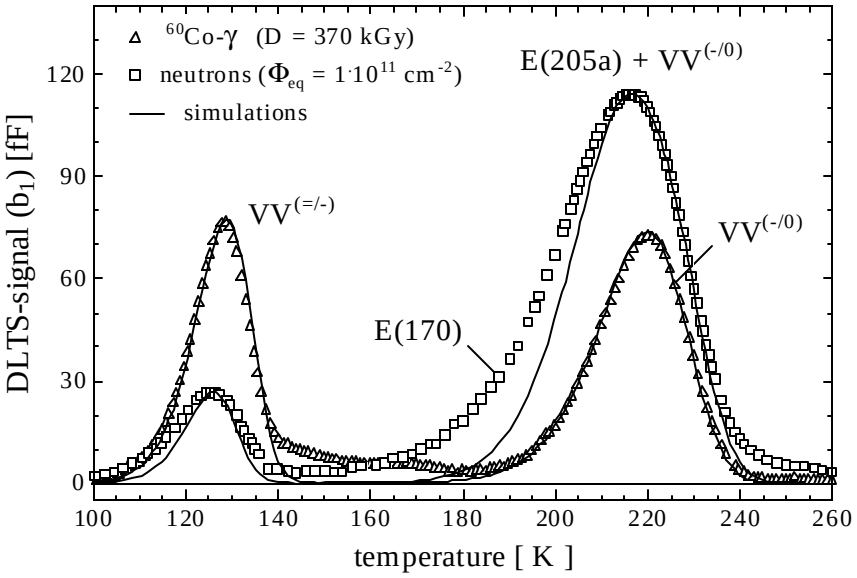

Fig. 35. Comparison of DLTS spectra after ^{60}Co-γ and neutron irradiation on identical samples (3 kΩcm) [14].

In addition to the qualitative differences between the DLTS spectra observed after ^{60}Co-γ and neutron-damage, heavy-particle damaged samples also display a unique annealing behaviour, compare Fig. 27. Two annealing steps at 70°C (E_C – 0.46 eV) and 170°C (E_C –0.40 eV) are now well established. The same annealing steps are observed in the leakage current annealing, proving that the cluster peak at about 205 K is a main contributor to the leakage current generation in heavy-particle damaged silicon.

Oxygen-Content Dependence of DLTS Spectra

Using the materials listed in Table 4, the effect that the Oxygen content has on the formation and annealing of radiation-induced defects has been studied. For this example, the samples were exposed to <5.3 MeV> neutrons at a Be(d,n) neutron generator. They were subsequently annealed at 60°C for 80 min. Fig. 36 shows the corresponding DLTS spectra. The introduction rate and the shape of the cluster peak at 205 K is found to be independent of the Oxygen concentration. This is expected, as it is known that the leakage current scales very nicely with the concentration of the cluster peak, and that the oxygen content does not affect the leakage current-related damage constant. To a first approximation the generation rate of VO_i (A-centre) defects does not depend on the oxygen concentration, since under the given irradiation conditions interstitial oxygen is the dominant sink for freely migrating vacancies. That means $[VO_i]$ is simply a measure of the total dose. Freely migrating silicon interstitials, on the other hand, are all converted into interstitial Carbon, which then has two reaction partners available to form stable defects: substitutional Carbon and interstitial Oxygen. Therefore the ratio between the two resulting reaction products $[C_iC_s]$ and $[C_iO_i]$ is proportional to the ratio between $[C_s]$ and $[O_i]$. This explains why for the oxygen-lean material a larger C_iC_s concentration is observed superimposing the VO_i peak. Finally we note the existence of Thermal Donors (TD), presumably a conglomerate of four oxygen atoms, in the CZ material. In principal these donors can also be created in oxygen-enriched float-zone material, and thus pose the danger of deteriorating the resistivity of the material. However, recipes to dissolve these donors and to circumvent their detrimental effects are well adopted within the silicon device processing industries.

Table 4. Materials used for the comparative DLTS study.

Material	Resistivity	Oxygen Content
ITME, FZ, n-type, <111>	120 Ωcm	$<5\times10^{16}$ cm^{-3}
ITME, FZ, n-type, <111>	800 Ωcm	1.7×10^{17} cm^{-3}
Polovodice, Cz, n-type, <111>	100 Ωcm	9×10^{17} cm^{-3}

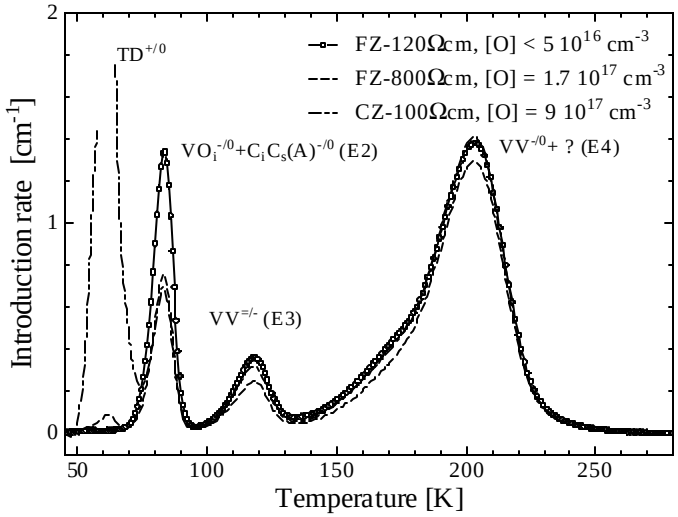

Fig. 36. DLTS spectra (normalised to introduction rate at 200K) obtained after irradiation with neutrons and a subsequent 80 min heat treatment at 60°C for different materials (see legend) [31].

Comparison of DLTS Spectra after Irradiation with Neutrons, Protons, Pions

A gradual transition from spectra characteristic of neutron damage to those characteristic of ^{60}Co-gammas is expected when one considers charged-particle damage with varying energies. At low charged-particle energy the relative importance of Coulomb scattering, imparting only small energies to the PKA, is increasing. The result of such a study is presented in Fig. 37, where <5.3 MeV> neutrons from a Be(d,n) generator, 192 MeV pions, and 27 MeV and 23 GeV protons have been used. The material (ITME FZ n-type, <111>, 800 Ωcm, jet-oxygenated, [O] = 1.7×10^{17} cm^{-3}) was the same in every case. Moreover, all samples were stored at 60°C for 80 min, in order to exclude any artefacts from differences in the annealing history.

Evidently, the cluster-peak at 205 K is introduced at the same rate in every case, reconfirming the intrinsic nature of the comprising defects and their location within the end-of-range region of the damage cascades. The introduction rate of the isolated point defects, represented by VO_i and C_iC_s, varies for the different particle types, in agreement with the expected enhancement due to Coulomb scattering. Here it is interesting to note that in this respect the very high-energetic (23 GeV) protons behave similarily to the 192 MeV pions.

Another striking observation concerns the peak normally assigned to the doubly-charged divacancy. Its variation with particle type resembles the one observed for the point defects. Also, quite obviously, the shape of the cluster peak at 205 K does not depend on the particle type. The broadening of the $VV^{-/0}$ transition and the apparent reduction of the apparent $VV^{--/-}$ concentration with respect to $VV^{-/0}$ can therefore not have the same origin. These observations need to be understood in terms of the lattice strain and the inter-centre charge transfer models.

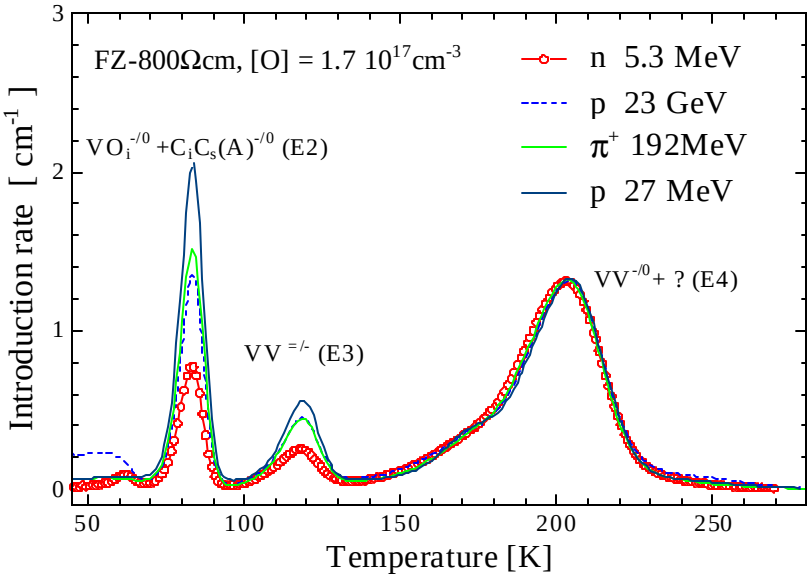

Fig. 37. DLTS spectra obtained on samples from the same wafer obtained after irradiation with different particles (see legend) and a 80 min lasting heat treatment at 60°C. The spectra are normalised to the 1 MeV neutron equivalent introduction rate at 200 K [31].

Correlation with Macroscopic Effects.

Short Term Annealing

It had been noted earlier that the activation energy for the short term annealing of the leakage current and the effective doping concentration are similar. Also it was known that the annealing at 70°C of the right-hand side broadening of the $VV^{-/0}$ transition, see Fig. 29, correlates with the leakage current annealing. It is therefore tempting to assume that the macroscopic effects have a common cause, namely, the deep level at E_C - 0.46 eV, and that this can be reasonably discussed on the grounds of simple Shockley-Read/Hall statistics. In order to substantiate this hypothesis, the deep level in question, labeled E4b in the following, was monitored during an isothermal annealing study at 60°C using DLTS, see Fig. 38. To obtain reliable defect parameters and concentrations for the annealing traps, the difference of two subsequent DLTS spectra was subjected to the standard DLTS evaluation procedure. The results are given in numerical form in Table 5. E4b was noted to be accompanied by a more shallow level at $E_C - 0.36$ eV (E4a), which, in analogy to the divacancy, tentatively can be considered a second ionization state of $E_C - 0.46$ eV (E4b). A very good correlation is observed between the change in leakage current between two annealing steps and the corresponding change in the concentration of E4b, see Fig. 39.

From the DLTS measurement, only the capture cross section for electrons σ_n is obtained. In order to calculate the leakage current from E4b using the Shockley/Read-Hall formulae, also the capture cross section for holes σ_p must be known. Vice versa, the measured leakage current can be exploited to obtain σ_p from such a calculation. Here we obtain a value of about 10^{-13} cm^2, which is quite conceivable. From forward current injection DLTS spectra it is in fact known that $\sigma_p > \sigma_n$. Using these parameters we can also calculate the contribution to the space charge from this trap. The value is however a factor five smaller than what is observed experimentally. Still, adjusting both cross sections σ_p and σ_n in order to account for the macroscopically observed effects gives $\sigma_n = 8.6\times10^{-15}$ cm^2 and $\sigma_p = 3.1\times10^{-13}$ cm^2, demonstrating that a comparatively small uncertainty of the cross section can have a big effect here. It should be noted that the

macroscopic measurements were carried out at room temperature whereas the DLTS data was gathered at about 200 K. Systematic studies on the temperature dependence of the cross sections and the trap ionization energy are needed to draw final conclusions.

Table 5. Defect parameters. The given introduction rates refer to certain annealing states at 60°C: (a) after 5 min and after 82000 min, (b) annealed in the period 5min to 10000 min and (c) after anneal to 82000 min.

Defect	ΔE_t [eV]	σ_n [cm^2]	Introduction rate [cm^{-1}]
E3	0.24	$\approx 10^{-14}$	0.24→0.41 (a)
E4a	0.36	$\approx 10^{-14}$	0.26 (b)
E4b	0.46	1×10^{-14}	0.62 (b)
E4	0.41	1.5×10^{-15}	1.04 (c)

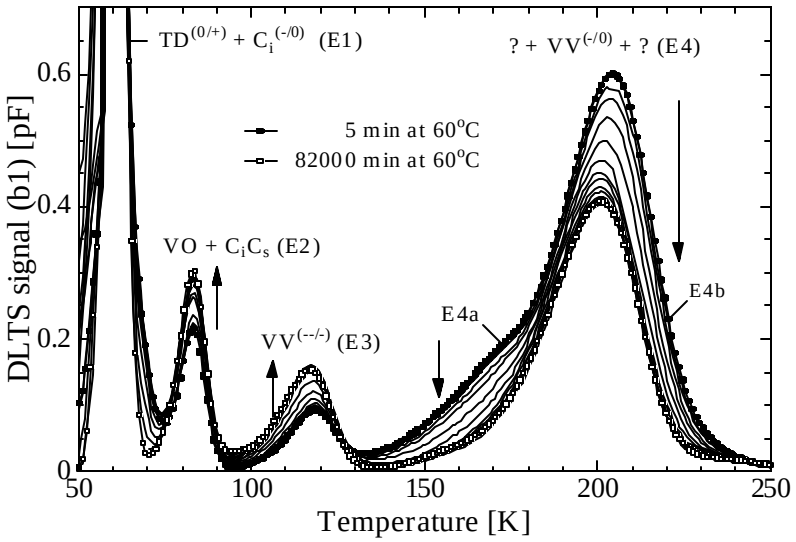

Fig. 38. Evolution of the DLTS spectrum at 60°C for a neutron irradiated sample produced from Cz silicon [31].

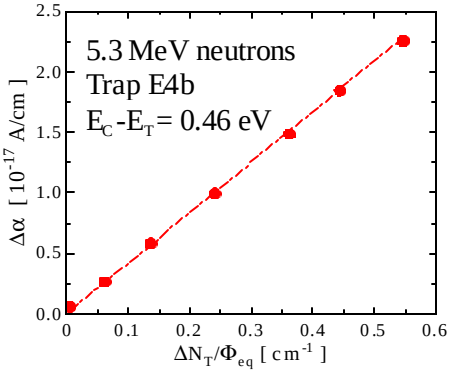

Fig. 39. Correlation between trap E4b and leakage current [31].

Reverse Annealing of the Effective Doping Concentration

So far, only a weak correlation between the W-line observed with PL, compare Fig. 34, and the change in doping concentration during the reverse annealing phase have been reported. A systematic isothermal annealing study at 80°C using TSC on a sample irradiated with 10^{13} cm^{-2} <5.3 MeV> neutrons has provided additional insight, see Fig. 40. The defect concentrations at the given fluence are too high to allow a quantitative analysis of the TSC spectra. Most importantly the spectra will exhibit a memory effect: a change in the peak signal at low temperature implies a change at all higher temperatures because of the variation of the space charge layer width with the concentration of ionised traps. It can still be argued that the signal H(116K) is indeed growing during the annealing sequence.

Fig. 41 demonstrates a good correlation between the integrated peak charge versus the change in space charge during the reverse annealing period. H(116K) had already previously been unambiguously connected with negative space charge by exploiting the bistability of this level. The simplest approach would mean that H(116K) is an acceptor level. This assignment would roughly be in agreement with the lower

limit of the concentration derived for this peak from the TSC spectrum. Moreover, for an acceptor level one would expect a fairly large capture cross section, because of the Coulombic attraction between the ionised acceptor and the emitted hole. Previously reported level parameters (ΔE_t = 0.32 eV and σ_p = 1.7×10^{-13} cm^2) would also match this criteria and could be reproduced here using C-DLTS, see Fig. 27. However, another set of parameters has been reported in ref. [14], which is surprisingly similar to the $C_i^{+/0}$ donor transition. Further studies are needed to ascertain the chemical nature of this defect.

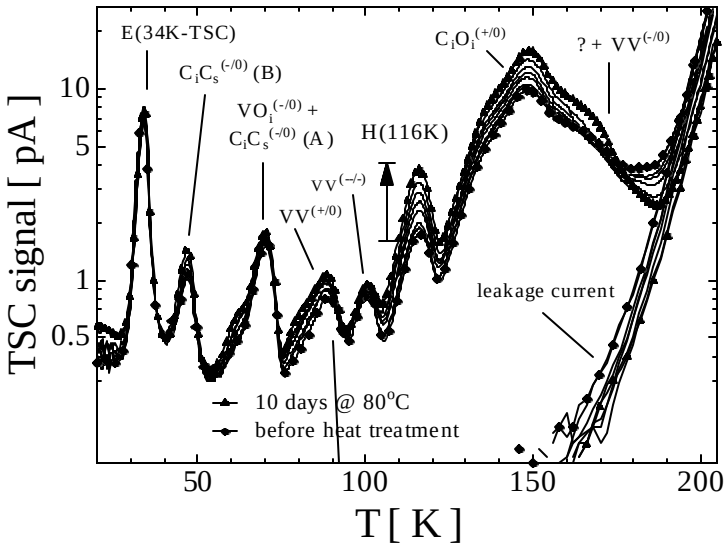

Fig. 40. Annealing of TSC spectra during the reverse annealing period [14].

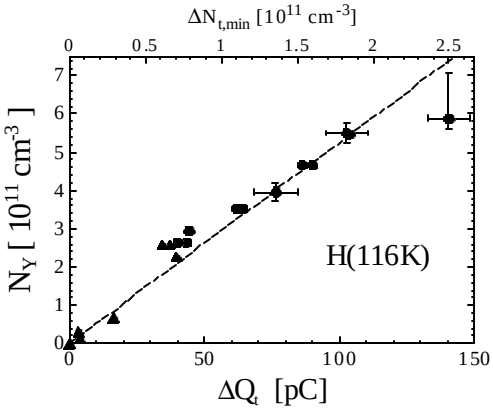

Fig. 41. Correlation between amount of reverse annealing and concentration of the trap H(116K).

7. MODELLING OF DEFECT PRODUCTION AND RADIATION DAMAGE

A key strategy of the ROSE Collaboration has been to understand macroscopic effects by using semiconductor device physics and known microscopic defect concentrations. A further ambitious aim has been to predict defect concentrations using defect kinetics models. This has been discussed in detail in previous status reports [1,2]. Consequently, only a brief summary will be given here together with recent modelling that explains why oxygen is beneficial to the radiation hardness of silicon when irradiated with protons. The defect kinetics model of Davies [32] has been adapted for detector material to predict defect concentrations after irradiation with ^{60}Co photons and fast hadrons. The reactions used in the model [33] are listed in Table 6. Reaction rates are controlled by the concentrations of impurities and their relative capture radii. Full details may be found in Ref. [33]. The input parameters required by the model are the oxygen and carbon impurity concentrations (determined by SIMS, IR absorption etc.) and the introduction rates of the primary defects. The rates used in the calculation are given in Table 7.

Table 6. Defect kinetics model reaction scheme.

Table 6A. Cluster reactions

I reactions	V reactions	C_i reactions
$I+V \rightarrow Si$	$V+V \rightarrow V_2$	.....

Table 6B. Diffusion reactions

$I+C_s \rightarrow C_i$	$V+V \rightarrow V_2$	$C_i+C_s \rightarrow CC$
$I+CC \rightarrow CCI$	$V+V_2 \rightarrow V_3$	$C_i+O \rightarrow CO$
$I+CCI \rightarrow CCII$	$V+O \rightarrow VO$	
$I+CO \rightarrow COI$	$V+VO \rightarrow V_2O$	
$I+COI \rightarrow COII$	$V+P \rightarrow VP$	
$I+VO \rightarrow O$		
$I+V_2O \rightarrow VO$		
$I+V_2 \rightarrow V$		
$I+VP \rightarrow P$		

Table 7. Introduction rates used in the modelling (refs. [34] and [35])

Radiation Source	V Introduction rate (cm^{-1})	V_2 Introduction Rate (cm^{-1})
^{60}Co gammas	2.7×10^{-4}	7.1×10^{-6}
1 MeV neutrons	0.58	0.96
24 GeV/c protons	0.61	0.46

In order to calculate device characteristics, the theory of Shockley, Read and Hall has been combined with the predicted defect concentrations. The states included in the SRH calculation of the effective doping, N_{eff}, and leakage current density, ΔJ_v, are listed in Table 8. It should be noted that there is some uncertainty in the energy level assignment of the divacancy-oxygen (V_2O) defect [36].

Table 8. Defect states considered in the SRH calculation.

Identity	Energy (eV)	Type	Charge
VO	E_c-0.17	Acceptor	(0/-)
V_2O	E_c-0.50±.05	Acceptor	(0/-)
V_2	E_v+0.20	Donor	(+/0)
	E_c-0.41	Acceptor	(0/-)
	E_c-0.23	Acceptor	(-/=)
VP	E_c-0.45	Acceptor	(0/-)
CO	E_v+0.36	Donor	(+/0)
CC	E_c-0.17	Acceptor	(0/-)

Gamma Irradiation

The predictions of the model for the evolution of N_{eff} during gamma irradiation are compared with experimental data from detectors with various oxygen concentrations in Fig. 42. The agreement between the model and data is impressive. The dominant contribution to N_{eff} arises from the V_2O state; an energy level of $E_{V_2O} = E_c$-0.54 eV is required to obtain agreement with the data, a value which lies within 1s of the experimental energy measurement. Oxygenated material is more radiation hard to gammas because V_2O production is suppressed by the competing reaction V + O → VO. The leakage current in these detectors has also been modelled. The V_2O defect dominates on account of its proximity to mid-gap. The model therefore suggests that a is reduced as the oxygen content rises, a prediction which has been borne out by experiment, ref. [37].

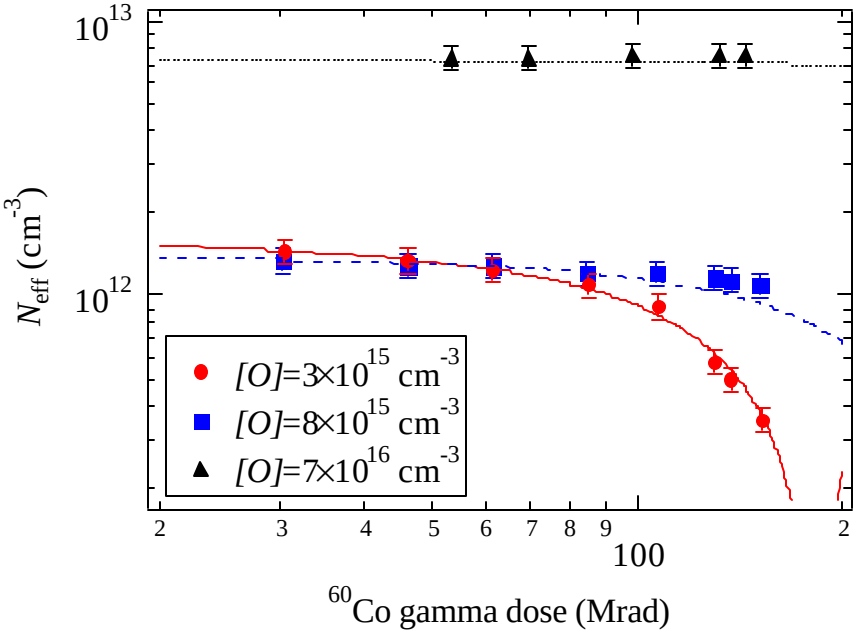

Fig. 42. Model predictions (lines) and experimental data (markers) for ^{60}Co gamma irradiation of samples with various oxygen concentrations and a carbon concentration of ~10^{16} cm-3.

Hadron irradiation

Using the value of E_{V_2O} fixed by the gamma data, the same modelling procedure was applied to the case of hadron irradiation. For 1 MeV neutrons, it was found that the predicted type inversion fluence was an order of magnitude higher than that observed experimentally. The dominant contribution to the doping changes predicted by the model again arose from the V_2O defect. The leakage current was underestimated by some 2 orders of magnitude. The potential errors in the model were examined carefully but could not possibly explain these discrepancies.

The presence of defect clusters in hadron-irradiated material, and their absence in gamma-irradiated material, suggests a possible cause. Several defects are strongly produced within the terminal clusters, including the divacancy (V_2) and two defects known as E70 and E170. The E70 state is multivalent, giving rise to acceptor levels at E_c-0.45 eV (0/-) and E_c-0.35 eV (-/=), whereas E170 gives rise to a single acceptor at E_c-0.37 eV (0/-) [38]. E70 and E170 are strongly correlated with annealing of the leakage current after irradiation, but neither state is sufficiently close to mid-gap to explain the magnitude of the observed current decrease in the conventional SRH picture [23].

Simple calculations indicate that the local density of V_2, E70 and E170 within the terminal clusters is of the order of 10^{19} cm^{-3}. It is evident, therefore, that some of these defects are close enough to exchange charge directly. There is compelling experimental evidence in the literature for such inter-centre charge transfer (see, for example, Ref. [39]). By writing general expressions for the rates of emission and capture between all levels of the V_2, E70 and E170 defects, and assuming equal carrier capture cross-sections throughout, it is possible to calculate the steady-state occupancy of each defect and the carrier generation rate numerically. The predicted value for the damage constant, a, which is the sum of the three components, is ~10×10^{-17} A.cm^{-1} in close agreement with what is actually observed.

The introduction rate of negative space charge is now ~5×10^{-3} cm^{-1}. To explain the experimental data, however, an introduction rate of ~25×10^{-3} cm^{-1} is required. Given that this preliminary calculation assumes equal carrier capture cross-sections, which is known not to be the case, it is not surprising that there is not a perfect agreement with the data. A more complete calculation is now in progress; from work to date it is evident that even small deviations from unity in the capture cross-section ratios can cause further enhancements in the introduction rate of negative space-charge. In order to make a step forward we have assumed that the total contribution of the clustered defects to the space charge is indeed of the order of ~25×10^{-3} cm^{-1} for 1 MeV neutrons and scales with the cluster defect introduction rates.

The results of combining the standard SRH calculation for point defects and the non-SRH calculation for clustered defects with this assumption are shown in Fig. 43 and Fig. 44. The plots show the predicted evolution of N_{eff} for various detector impurity concentrations for 1 MeV neutrons and 24 GeV protons respectively. The experimental data are described well. There are several points to note. In the case of neutron irradiation, the various detectors display similar radiation tolerance; the only differences observed are due to differences in the initial resistivity of the devices. In the case of proton irradiation, however, the oxygen-enriched detector is more rad-hard and the carbon-enriched detector less rad-hard than the standard device. The reason for this is that, in the case of proton irradiation, the primary introduction rate of the vacancy is proportionally larger than in the case of neutron irradiation. Hence, the role played by V_2O in determining N_{eff} is greater for protons. As in the case of gamma irradiation, a high oxygen concentration suppresses V_2O production and thus the changes in N_{eff}. Conversely, a high carbon concentration encourages V_2O production because substitutional carbon acts as a sink for interstitials and suppresses capture of interstitials at V_2O itself and its pre-cursor states (Table 6).

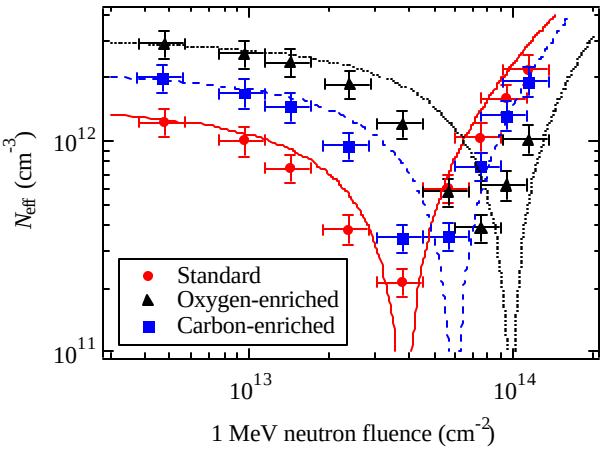

Fig. 43. Model predictions (lines) and experimental data (markers) for 1 MeV neutron irradiation. Circles - *[O]* = 3×10^{15} cm^{-3}, *[C]* = 5×10^{15} cm^{-3}; triangles - *[O]* = 1.7×10^{16} cm^{-3}, *[C]* < 2×10^{16} cm^{-3}; squares - *[O]* < 5×10^{16} cm^{-3}, *[C]* = 1.8×10^{16} cm^{-3}.

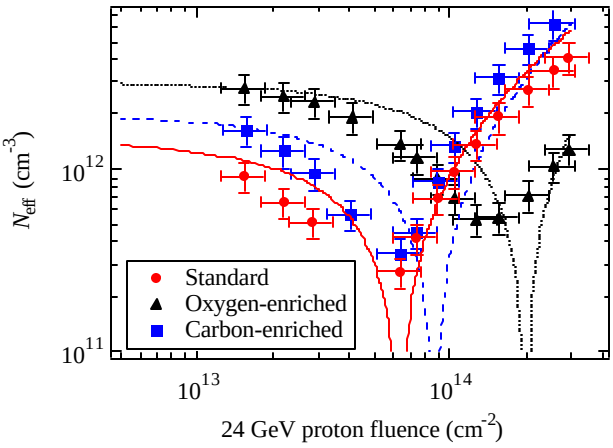

Fig. 44. Model predictions (lines) and experimental data (markers) for 24 GeV proton irradiation. Circles - *[O]* = 3×10^{15} cm^{-3}, *[C]* = 5×10^{15} cm^{-3}; triangles - *[O]* = 1.7×10^{16} cm^{-3}, *[C]* < 2×10^{16} cm^{-3}; squares - *[O]* < 5×10^{16} cm^{-3}, *[C]* = 1.8×10^{16} cm^{-3}.

It follows that it is misleading to compare the results of radiation damage studies by simply scaling N_{eff} data with the hardness factor of the source. The figures which determine radiation hardness are the actual defect introduction rates themselves, which do not necessarily scale with NIEL.

Summary

The changes in N_{eff} and dark current during gamma irradiation have been modelled satisfactorily in terms of production of the V_2O defect. In the case of hadron irradiation, electrical characteristics are controlled by cluster defects, with a contribution to N_{eff} from the V_2O state. The V_2O defect is more copiously produced during proton irradiation on account of the proportionally higher vacancy introduction rate, hence the radiation hardness of materials to protons is more sensitive to impurity concentrations than in the case of neutrons. This modelling can be considered to be indirect evidence for the presence of V_2O. Direct experimental evidence for V_2O has yet to be obtained. There is evidence for a deep level close to mid-gap from TCT data but its precise nature has not been determined. Quantum mechanical modelling of this defect predicts that it is an acceptor close to mid-gap [40].

8. OUTLOOK AND OPEN PROBLEMS

The RD48-Collaboration has achieved significant results and reached its original goal to develop radiation hard silicon detectors and provide guidelines to the LHC experiments. However, there are still some remaining issues both at a practical and fundamental level that need to be resolved. These are addressed in this section.

Final optimisation of the radiation hardening effect of oxygen enrichment

To date, experiments have been performed with a variety of different oxygenation processes from a 16h diffusion at 1150°C up to 9 days at 1200°C (see Table 9). The Quartz ovens used at the detector manufacturers do not allow a higher temperature than 1150°C. Even at this temperature the lifetime of the quartz tubes is limited and hence replacement adds to the price of detector production. Furthermore, safety requirements may prohibit continuous operation of the ovens for a 24hr/day basis. For all these reasons, the diffusion process should be minimised without losing the advantages that oxygenation has on the radiation hardness. In the last year, much has been done to systematically study this process. However, there are still some open questions regarding the minimum diffusion process required not only to maintain the hardening for the stable damage effect but to also to control reverse annealing. The fact that reverse annealing can be affected by high oxygen levels was unexpected but very welcome. As this effect has important consequences for the maintenance periods used by the experiments, progress in this area needs urgent further investigation. These measurements take a long time and results will only become available over the next few months. Another open question which can only be tackled together with the detector manufacturers will be the not yet understood variations seen in standard control diodes and their possible relation to different manufacturing techniques. Material characterisation and the measurement of the complete set of damage parameters needs to be performed for each manufacturer.

Consistency of the RD48 results on diodes with pixel- and strip detectors

Most of the RD48-results presented in this report have been obtained using special ROSE test detectors, i.e. small pad diodes with usually just one guard ring. The geometry of the real strip and pixel-detectors differs appreciably from this simple structure. They have a much more complex surface geometry with SiO_2 between the individual strips or pixels and employ complex guard-ring structures. The few measurements that have been made on full-scale detectors show an acceptable agreement with simple test diodes. We see no reason for considerable deviation between the strip and diode results, nevertheless, the consistency of the RD48 results on diodes should be carefully tested against full-scale detectors. This task has already started and a close direct collaboration between the CERN-MIC-SD group of RD48 and the large LHC experiments has been initiated. Two joint meetings have already been held and RD48 diodes have been used in parallel with LHC detectors during irradiation experiments. For instance, prototype ATLAS strip detectors have been irradiated together with our own diodes. These consistency checks will be pursued further both with ATLAS and CMS.

Table 9.: Material produced under the auspices of the ROSE-collaboration in 1999. Diode Producers: BNL: Brookhaven National Lab, Upton NY, USA; Sintef: Sintef, Oslo, Norway; CIS: CIS, Erfurt, Germany; ST: STMicroelectronics, Catania, Italy.

Producer diode	**Producer silicon**	**Orientation**	**Resistivity [kΩcm]**	**Treatment (Oxygenation)**	**SIMS (150 mm) [O] [cm^{-3}]**
BNL	Topsil	<100>	1.0	9d in N_2 1200°C	4e17
CIS	Topsil	<100>	1.0	9d in N_2 1200°C (performed at BNL)	3.4e17
CIS	Topsil	<100>	1.3	no diffusion step	2.2e16
CIS	Wacker	<111>	3.9	no diffusion step	< 1e16
CIS	Wacker	<111>	4.4	16h in N_2 at 1150°C	1.4e17
CIS	Wacker	<111>	4.0	24h in N_2 at 1150°C	3.0e17
Sintef	Wacker	<111>	2	72h in N_2 at 1150°C	1.5-2e17
Sintef	Wacker	<111>	2	72h in O_2 at 1150°C; oxide thinning	1.5-2e17
Sintef	Wacker	<111>	2	72h in O_2 at 1150°C; oxide removal + reoxidation	1.5-2e17
Sintef	Topsil	<111>	6	72h in N_2 at 1150°C	1.5-2e17
Sintef	Topsil	<111>	6	72h in O_2 at 1150°C; oxide thinning	1.5-2e17
Sintef	Topsil	<111>	2	72h in O_2 at 1150°C; oxide removal + reoxidation	1.5-2e17
ST	Wacker	<111>	1.0	30h in N_2 at 1200°C; (SiC-oven)	-
ST	Wacker	<100>	1.1	30h in N_2 at 1200°C; (SiC-oven)	-
ST	Wacker	<111>	1.0	60h in N_2 at 1200°C; (SiC-oven)	-
ST	Wacker	<100>	1.0	60h in N_2 at 1200°C; (SiC-oven)	-
ST	Wacker	<111>	2.2	30h in N_2 at 1200°C; (SiC-oven)	-
ST	Wacker	<100>	2.4	30h in N_2 at 1200°C; (SiC-oven)	-
ST	Wacker	<111>	2.0	60h in N_2 at 1200°C; (SiC-oven)	-
ST	Wacker	<100>	2.4	60h in N_2 at 1200°C; (SiC-oven)	-
ST	Wacker	<111>	16	30h in N_2 at 1200°C; (SiC-oven)	-
ST	Wacker	<100>	15	30h in N_2 at 1200°C; (SiC-oven)	-

The charged hadron-neutron puzzle and its consequences for LHC

Many experiments in recent years have shown that to compare bulk damage parameters for radiation sources using different particle types and energy one should scale results using the Non-Ionising Energy Loss (NIEL). This important result enables one to extrapolate results obtained with particular sources to the complex particle and energy spectra that will be encountered in the LHC experiments by appropriate scaling using the NIEL data. It was completely unforeseen that this assumption, which had been proven to be valid for standard material, was incorrect for high energy proton or pion irradiation of oxygen enriched silicon. It has been proposed that the origin of this difference can be understood by a more detailed study of NIEL. Neutrons in the energy range up to several MeV only interact with the silicon by elastic scattering, resulting in high energy recoil Si-atoms. However, charged hadron interactions incorporate a considerable contribution due to Coulomb scattering resulting in low energy recoils. Assuming that recoil atoms below a certain energy (5 keV) cannot produce defect clusters but predominantly point defects, one would expect that for charged hadrons much of the total NIEL contributes to impurity related defects which leads to the hardening effect of oxygen. This is consistent with results from microscopic studies (see Fig. 37 and comments in Section 6), which show that there are more diffusing vacancies and interstitials for protons and pions. Section 7 shows that device modelling is also consistent with this hypothesis.

Fig. 45 shows results from a detailed study of NIEL versus the silicon atom recoil energy for different particles [41]. Only elastic scattering (both nuclear and Coulomb) has been included. The functional dependence shown in Fig. 45 also supports the above stated assumption. The relative NIEL contribution for recoil

energies lower than 5 keV is negligible for 1 MeV neutrons. However, a considerable portion of the NIEL for charged hadrons exists in that energy regime. One can argue that elastic scattering of high energy pions or protons contributes only 30 (200 MeV pions) to 37% (9 GeV protons) of the total NIEL and that therefore according to Fig. 45 the net contribution from recoils below 5 keV is only 6 to 10%. Hence it is hard to believe that this small value could lead to the observed effect. However, for high energy particles there are many higher order nuclear reactions which lead to a variety of secondary reaction products which again interact with the Si-atoms partly by the Coulomb interaction and hence give rise to a significant number of low energy recoils. More detailed investigations using Monte Carlo simulations are necessary. However one result is already apparent: at high energies, nuclear reactions induced by charged hadrons and neutrons are practically the same. Thus, the secondary Coulomb contribution to low energy recoils in the silicon lattice can also be expected following high energy neutron damage.

Fig. 46 shows the main contributions to the energy spectra present in the inner detector of the ATLAS experiment folded with the appropriate damage efficiency for the neutron and pion contribution [42]. While the pion spectrum is centred around 200 MeV, neutrons show an almost homogeneous energy distribution between 0.1 and 100 MeV. From the arguments outlined above, at least the high energy part of the neutron spectrum could therefore also lead to low energy recoils and thus the damage produced by them would partly result in the same behaviour as observed for protons. However, all test experiments with neutrons performed so far would have not shown this effect because the energy spectra extended only to about 10 MeV. In most cases reactor neutrons were used.

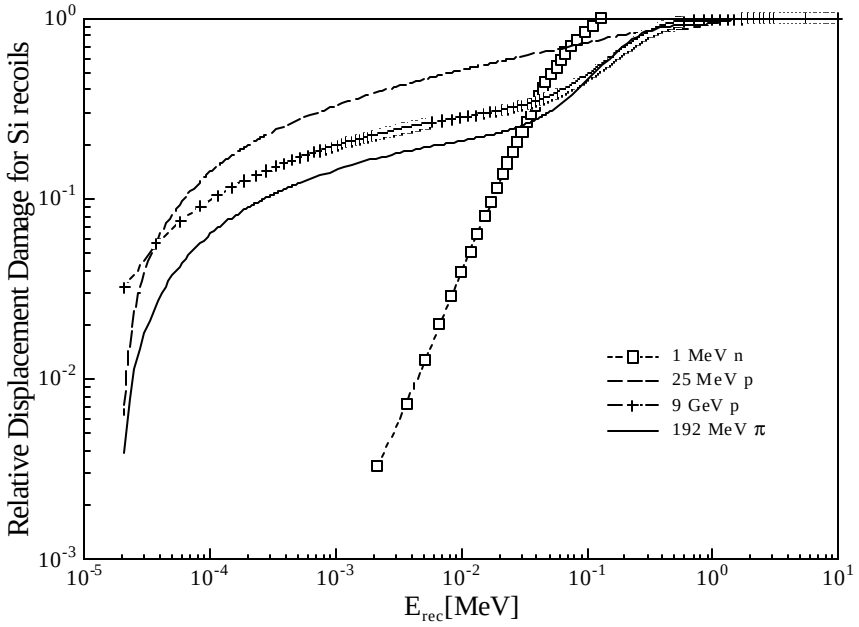

Fig. 45. Relative damage efficiency for different particles as function of recoil energy.

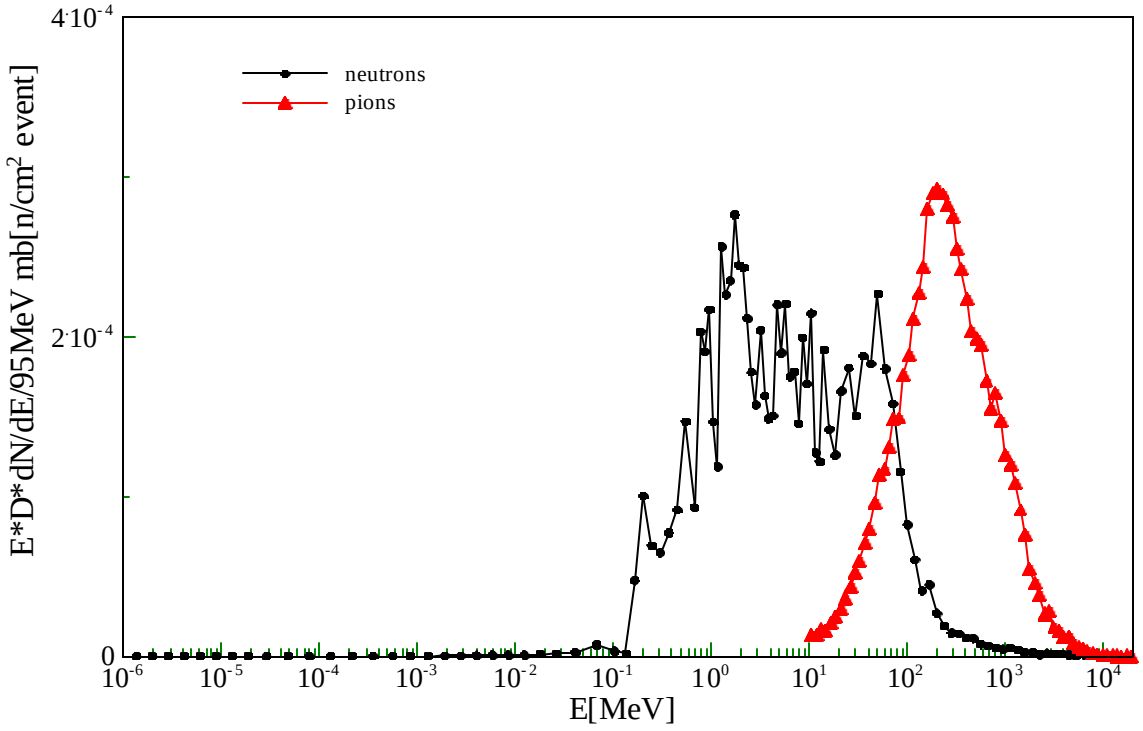

Fig. 46. Neutron and pion energy spectrum folded with NIEL as present in ATLAS-SCT.

An important consequence of these considerations is the necessity for dedicated test experiments employing radiation fields which more closely resemble the LHC environment. The particle sources best suited for this project are the PSI facility for 200 MeV pion irradiation and the neutron shuttle, which was recently installed at the CERN-PS [13]. In fact the spectral distribution, displayed in Fig. 47, reproduces the LHC neutron spectrum in the inner detector very well - compare with Fig. 46.

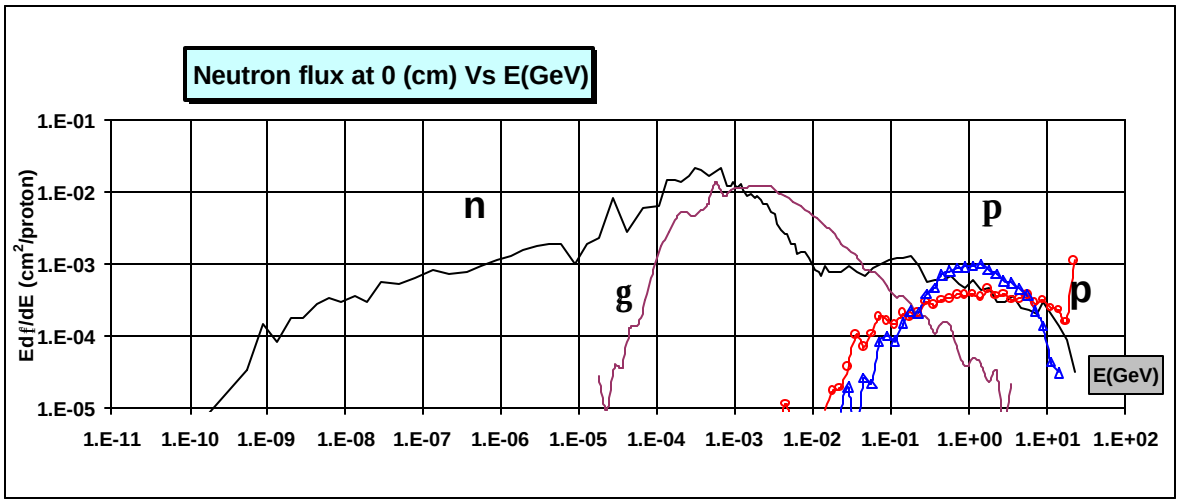

Fig. 47. Energy spectra of neutrons, pions, protons and gammas in the beam axis of the IRRAD2 cavity in the CERN PS East Hall [13].

REFERENCES

[1] RD48 Status Report, CERN/LHCC 97-39, June 1997.
[2] RD48 Status Report, CERN/LHCC 98-39, October 1998.
[3] ROSE Collaboration Proposal, CERN/LHCC 96-23, P62/LHC R&D, April 1996.
[4] 2nd ROSE Workshop Internal Report, February 1997.
[5] 3rd ROSE Workshop, DESY-Proceedings-1998-02, February 1998.
[6] 4th ROSE Workshop, CERN/LEB 98-11, December 1998.
[7] ROSE Meeting, CERN 14-15 June 1999, CERN/LEB 99-8.
[8] ROSE Web Page – http://www.brunel.ac.uk/research/rose/
[9] Z.Li et al., IEEE Trans. Nucl. Sci. NS-39, No. 6, (1992), p. 1730-1738.
[10] B. Svensson et al., J. Appl. Phys. 72, 5616 (1992).
[11] B. Dezillie et al., "The Effect of Oxygen Impurities on Radiation Hardness of FZ Silicon Detectors for HEP after Neutron, Proton and Gamma Irradiaion", Subm. to IEEE-NS.
[12] A.Vasilescu in Ref. [5] and http://sesam.desy.de/~gunnar/
[13] M. Glaser et al., "Radiation Test Facilities in the New PS East Hall at CERN", to be published.
[14] M. Moll, Ph.D thesis, University of Hamburg, 1999, DESY-THESIS-1999-040.
[15] M.Moll et al., NIMA 426 (1999) 87.
[16] F. Lemeilleur, G. Casse, M. Glaser, A.Ruzin, CERN EP-MIC-SD
[17] A. Ruzin et al., presented on the Vertex 1999 conference, to be published in NIMA.
[18] G. Lindstroem, M.Moll, E.Fretwurst. NIMA 426 (1999) 1, and literature cited there.
[19] Data provided by G.Casse, Liverpool, (see also http://hep.ph.liv.ac.uk:80/~gcasse/).
[20] E. Gregoriev et al., presented on the 4th ROSE Workshop, Ref. [6] page 648.
[21] C. Becker, C. Goessling, C. Lichau, T. Wuebben, J. Wuestenfeld, R. Wunstorf "Gate-controlled diodes for characterization of the Si-Sio2 interface with respect to surface effects of silicon detectors." accepted for punlication in Nuclear Instruments & Methods.
[22] B.G. Svensson et al., Phys. Rev. B 43 (3), 2292 (1991).
[23] S.J. Watts et al., IEEE Trans. Nucl. Sci. 43 (6), 2587 (1996).
[24] H. Feick, presented on the 4th ROSE Workshop, Ref. [6], page 503.
[25] Z. Li et al., IEEE Trans. NS 43, 1590 (1996).
[26] E. Verbitskaya, St Petersburg, Ioffe Physico-Technical Institute, Russia, private comm.
[27] I. Pintilie, Bucharest, Institute of Physics and Technology of Materials, Romania, private comm.
[28] Z. Li et al., Nucl. Instr. & Meth. A388, 297 (1997).
[29] E. Fretwurst et al., Nucl. Instr. & Meth. A388, 356 (1997).
[30] H. Feick and E.R. Weber, Paper presented at the 20th International Conference on Defects in Semiconductors ICDS-20, July 26–30, 1999, Berkeley, CA, USA, to be published in Physica B.
[31] E .Fretwurst et al., paper submitted to the "First International Workshop on Defect Engineering of Advanced Semiconductor Devices" of the ENDEASD, held in Santorini -Greece, 21-22 APRIL 1999, accepted for publication in Materials Science in Semiconductor Processing.
[32] G. Davies et al., Semicond. Sci. Technol. 2 (1987) 524.
[33] K. Gill et al., J. Appl. Phys. 82 (1997) 126.
[34] S. J. Watts et al., CERN/LEB 98-11 (1998) 432.
[35] M. Moll et al., Nucl. Instr. & Meth. A 388 (1997) 335.
[36] Y. H. Lee et al., Radiat. Eff. 29 (1976) 7.
[37] E. Fretwurst et al., CERN/LEB 98-11 (1998) 221.
[38] M. Ahmed, PhD Thesis Brunel University (1998).
[39] A. Frens et al., Phys. Rev. Lett. 72 (1994) 2939.
[40] R. Jones et al, Proceedings of 1st ENDEASD Workshop, Santorini, April 1999.
[41] A. Vasilescu and M. Huhtinen, work in progress.
[42] A. Vasilescu, ROSE/TN/97-2.